Boundary-Layer Meteorol (2009) 133:189–217
DOI 10.1007/s10546-009-9427-x

ARTICLE

Turbulent Pressure and Velocity Perturbations Induced by Gentle Hills Covered with Sparse and Dense Canopies

Edward G. Patton · Gabriel G. Katul

Received: 3 December 2008 / Accepted: 10 September 2009 / Published online: 26 September 2009

Abstract How the spatial perturbations of the first and second moments of the velocity and pressure fields differ for flow over a train of gentle hills covered by either sparse or dense vegetation is explored using large-eddy simulation (LES). Two simulations are investigated where the canopy is composed of uniformly arrayed rods each with a height that is comparable to the hill height. In the first simulation, the rod density is chosen so that much of the momentum is absorbed within the canopy volume yet the canopy is not dense enough to induce separation on the lee side of the hill. In the second simulation, the rod density is large enough to induce recirculation inside the canopy on the lee side of the hill. For this separating flow case, zones of intense shear stress originating near the canopy-atmosphere interface persist all the way up to the middle layer, 'contaminating' much of the middle and outer layers with shear stress gradients. The implications of these persistent shear-stress gradients on rapid distortion theory and phase relationships between higher order velocity statistics and hill-induced mean velocity perturbations (Δu) are discussed. Within the inner layer, these intense shear zones improve predictions of the spatial perturbation by K-theory, especially for the phase relationships between the shear stress ($\sim \partial \Delta u/\partial z$) and the velocity variances, where z is the height. For the upper canopy layers, wake production increases with increasing leaf area density resulting in a vertical velocity variance more in phase with Δu than with $\partial \Delta u/\partial z$. However, background turbulence and inactive eddies may have dampened this effect for the longitudinal velocity variance. The increase in leaf area density does not significantly affect the phase relationship between mean surface pressure and topography for the two simulations, though the LES results here confirm earlier findings that the minimum mean pressure shifts downstream from the hill crest. The increase in leaf area density and associated flow separation simply stretches this difference further downstream. This shift increases the pressure drag, the dominant term in the overall drag on the hill surface, by some

E. G. Patton (✉)
National Center for Atmospheric Research, P.O. Box 3000, Boulder, CO 80307-3000, USA
e-mail: patton@ucar.edu

G. G. Katul
Nicholas School of the Environment & Department of Civil and Environmental Engineering,
Duke University, Durham, NC 27708-0328, USA

15%. With regards to the normalized pressure variance, increasing leaf area density increases σ_p/u_*^2 near the canopy top, where u_* is the longitudinally averaged friction velocity at the canopy top and σ_p is the standard deviation of the pressure fluctuations. This increase is shown to be consistent with a primitive scaling argument on the leading term describing the mean-flow turbulent interaction. This scaling argument also predicts the spatial variations in σ_p above the canopy reasonably well for both simulations, but not inside the canopy.

Keywords Canopy turbulence · Flow over hills · Large-eddy simulation · Rapid distortion theory · Reversed flow · Turbulent pressure

1 Introduction

The problem of how gentle hills perturb the mean flow and the pressure field far from a rough surface has been extensively studied (Jackson and Hunt 1975; Hunt et al. 1988; Gong and Ibbetson 1989; Ying and Canuto 1996; Gong et al. 1996; Kim et al. 1997; Belcher and Hunt 1998; Taylor 1998; Henn and Sykes 1999; Wood 2000; Brown et al. 2001; Athanassiadou and Castro 2001; Ayotte and Hughes 2004; Wagner et al. 2007; Poggi et al. 2007). In comparison, how gentle hills perturb the bulk flow within the canopy sublayer has received much less attention. Recent theoretical progress (Finnigan and Belcher 2004; Poggi et al. 2008), hereafter referred to as FB04, flume experiments (Poggi and Katul 2007a,b,c, 2008), hereafter referred to collectively as PK07, first-order closure modelling (Ross and Vosper 2005), hereafter referred to as RV05, and large-eddy simulations (LES) (Tamura et al. 2007; Ross 2008; Dupont et al. 2008) are beginning to fill some of this knowledge gap. The motivation for exploring the latter problem are numerous and are often linked to: (1) quantifying biosphere-atmosphere exchange of trace-gas fluxes and other scalars from tall vegetation situated on complex terrain, including footprint determination (Raupach et al. 1992; Raupach and Finnigan 1997; Grace and Malhi 2002; Schmid 2002; Aubinet et al. 2003; Feigenwinter et al. 2004; Staebler and Fitzjarrald 2004; Aubinet et al. 2005; Katul et al. 2006); (2) modelling heavy-particle dispersion (e.g. seed and pollen) when exploring the re-colonization of disturbed areas within forests (Nathan et al. 2002; Katul et al. 2005; Nathan and Katul 2005), control of pests, gene flow and its implications for both ecosystem composition or designs of biocontainment zones (Williams et al. 2006); (3) assessing how the presence of a tall canopy affects siting choices for wind turbines on hills for optimal energy capture; (4) deriving wind loads on buildings (Bitsuamlak et al. 2004, 2006); (5) the need to represent the combined effect of the vegetation-hill system via an effective roughness or drag coefficient in mesoscale and numerical weather prediction models (Xu and Taylor 1995; Belcher and Wood 1996; Belcher and Hunt 1998; Salvetti et al. 2001; Beljaars et al. 2004; Vosper and Brown 2007), to name a few. However, much of these applications cannot be addressed by only tracking how hills perturb the mean flow properties; they require knowledge of how the combined canopy-hill system alters higher order statistics such as velocity variances, turbulent stresses, and in some cases pressure variances.

The original framework of Jackson and Hunt (1975) for dividing the flow above the hill into different layers (e.g. outer versus inner layers) and the revisions proposed by FB04 thereafter to include a canopy sublayer provide some clues about the mechanisms governing the variability in turbulent intensities, at least in terms of phase relationships relative to the hill surface. Rapid distortion theory (RDT) provides an organizing framework to analyze the higher-order flow statistics in the outer layer (Britter et al. 1981; Hunt and Carruthers 1990; Belcher and Hunt 1998; Athanassiadou and Castro 2001), while K-theory, with the

appropriate choice of mixing length scales, provides an organizing framework for analyzing these phase relationships in the inner layer (as in FB04). How the canopy modifies this emerging picture for second-order statistics (including pressure variance) and their phase relationship to the hill surface was not explored in FB04. Understanding the response of first- and second-order moments to variations in canopy density is an essential step toward the interpretation of observations taken in this regime and in the development of simpler models attempting to represent the impact of varying canopy types on turbulent exchange in larger-scale models that are unable to resolve the vegetation, the orography, or their interaction.

Hence, our study analyzes two LES experiments simulating turbulence over a train of gentle hills mimicking the cosine hill surface in the flume experiments described by PK07. The hill surface in both calculations is covered with a canopy composed of uniformly arrayed rods, where the rod height is comparable to the hill height. In the first simulation, the rod density is chosen so that much of the momentum is absorbed within the canopy volume yet not too dense to induce recirculation on the lee side of the hill (hereafter referred to as the *non-separating* case). In the second simulation, the rod density is sufficiently large to induce recirculation within the canopy volume (here after referred to as the *separating* case). These two runs, identical in all respects except for the canopy density, are likely to produce different interaction regimes between the flow in the outer layer (that dictates surface pressure gradients) and topography. Phase shifts and asymmetry between the topography and the ground pressure, which can be modified by the recirculation zone, further affects these phase relationships between the second-order flow statistics and the hill surface as well as the overall drag acting on the hill surface.

2 Scaling Analysis and Dynamical Regions

2.1 Background States

For flow over gentle hills, the mean velocity $\bar{U}$ is expressed as

$$\bar{U}(x,z) = U_b(z) + \Delta u(x,z), \tag{1}$$

where the background state U_b is often defined as the upstream velocity far from an isolated hill, and $\Delta u(x,z)$ is the hill-induced perturbation from this background state. In FB04, the background states are expressed as:

$$U_b(z) = \frac{u_{*,b}}{k_v} \log\left(\frac{z-d}{z_o}\right), \quad z \geq h_c \tag{2a}$$

$$U_b(z) = U_{h,b} \exp\left(\frac{\beta}{l}(z-h_c)\right), \quad z < h_c, \tag{2b}$$

where h_c is the canopy height, $k_v = 0.4$ is the von Karman constant, u_* is the friction velocity, d is the zero-plane displacement, z_o is the aerodynamic roughness length of the canopy, $U_{h,b}$ is the mean background velocity at $z = h_c$, $\beta = u_{*,b}/U_{h,b}$, $l = 2\beta^3 L_c$ is a constant effective mixing length inside the canopy, $L_c = (C_d a)^{-1}$ is the adjustment length scale that varies with the canopy drag (C_d) and the leaf area density (a). To ensure continuity of the mean velocity profile at $z = h_c$, $d = h_c - l/k_v$ and $z_o = d\, e^{-k_v/\beta}$.

When considering flows over a train of gentle hills instead of an isolated hill, the background state may not be well represented by the upstream mean velocity profile (Ayotte 1997). The upstream velocity prior to the nth hill is different from the upstream velocity

colliding with the ($n^{th} - 1$) hill. Hence, for a train of gentle hills, it is convenient to define a different 'background' state. Following similar arguments as those discussed in PK07, the longitudinal average along the hill wavelength is selected. Hereafter, the subscript b indicates this background state. This definition is especially useful for the simulations presented here because periodic boundary conditions are used (a convenient method to obtain turbulent inflow conditions) implying that the computationally generated flow resembles that which has encountered an infinitely repeating train of hills. Comparisons between the background states predicted by Eq. 2 and estimated from longitudinal averaging of the LES results are discussed later.

2.2 Scaling Regimes

Early analysis of boundary-layer flows over gentle hills decomposed the boundary layer into two distinct layers known as the outer and inner layers after Jackson and Hunt (1975), hereafter referred to as JH75. These two layers emerged from time-scale arguments associated with the relative adjustment of the mean and turbulent flows to topographic perturbations. In particular, the mean distortion and Lagrangian integral time scales (T_D and T_L, respectively) are commonly employed to explore how the mean flow and turbulence adjust to topographic variations within these two regions. T_D characterizes the distortion of turbulent eddies due to the straining motion associated with the spatial variability in the mean flow caused by the hill. It represents the characteristic time that the mean flow field needs to stretch and destroy large eddies through work done by advection against the mean spatial velocity gradients.

An estimate of T_D can be obtained from (Belcher and Hunt 1998),

$$T_D = \frac{L}{\bar{U}} = \frac{L}{U_b + \Delta u} = \frac{L}{U_b}\left(1 + \frac{\Delta u}{U_b}\right)^{-1} \approx \frac{L}{U_b}\left(1 - \frac{\Delta u}{U_b}\right). \tag{3}$$

T_L characterizes the time scale of classical turbulent stretching (or relaxation) of large eddies due to the action of a local mean velocity gradient. Stated differently, T_L is the time that turbulent fluctuations need to come to equilibrium with the local mean velocity gradient, and this can be estimated from

$$T_L = \frac{u_*^2}{\varepsilon} = \frac{u_*^2}{-\overline{u'w'}(\partial \bar{U}/\partial z)} = \frac{u_*^2}{(u_*^3/k_v z)} = \frac{k_v z}{u_*} = \frac{k_v z}{u_{*b}\,(1 + (\Delta u_*/u_{*b}))}, \tag{4}$$

where ε is the mean turbulent kinetic energy dissipation rate (assumed to balance shear production only for scaling purposes). Hence, to first order,

$$T_L \approx \frac{k_v z}{u_{*b}}\left(1 - \frac{\Delta u_*}{u_{*b}}\right) \approx \frac{k_v z}{u_{*b}}\left(1 + \left(\frac{K_{t,b}}{u_{*b}}\right)\frac{\partial \Delta u}{\partial z}\right), \tag{5}$$

where K_t is the turbulent diffusivity.

These arguments suggest that T_D scales with Δu, while T_L scales with $\partial \Delta u/\partial z$. The ratio T_D/T_L can be used to separate the outer from the inner layer, as briefly discussed below. A thorough review of these arguments can be found elsewhere (Belcher and Hunt 1998). Figure 1 summarizes the key terms in the mean momentum balance and the scaling arguments (velocity or time scales) for each of the layers across the hill, discussed next.

2.3 Outer Layer

In the layer where $T_D/T_L \ll 1$, the local stretching of large eddies is much slower than the distortion due to advection. This layer is called the *rapid-distortion* layer or the outer layer

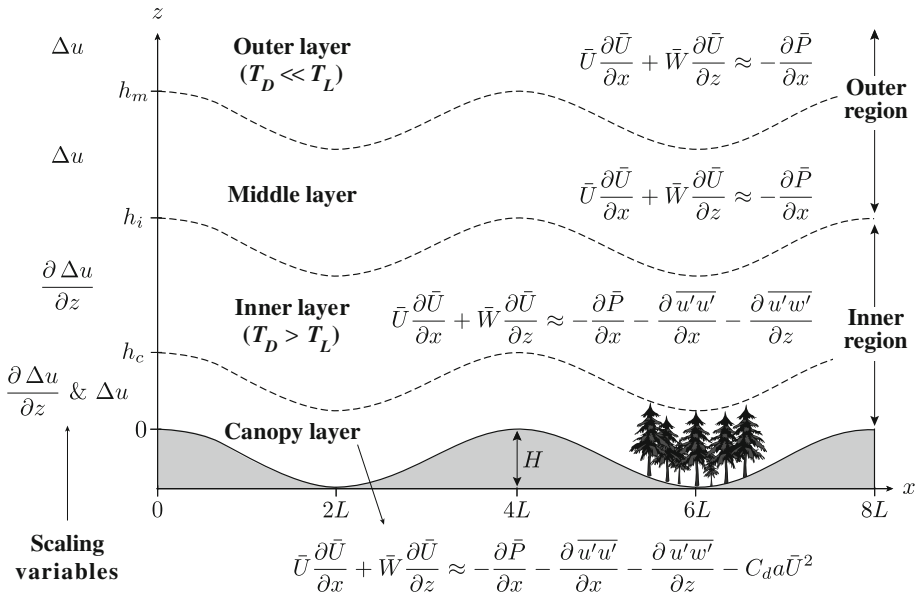

Fig. 1 Schematic diagram defining the length scales, layers and regions. For each layer, the key terms in the mean momentum balance above the hill surface and the scaling variables for velocity or time are depicted. RDT scaling (i.e. Δu) is expected to hold in the outer (inviscid) and middle (inviscid but rotational) layers, where the mean distortion time scale (T_D) is much smaller than the Lagrangian time scale (T_L). The K-theory and shear-stress scaling (i.e. $\partial \Delta u/\partial z$) are expected to hold in the inner layer where $T_D > T_L$. The quantities on the left represent the scaling variables for velocity or time. The emergence of Δu as a velocity scale inside the canopy is not connected to RDT and is presumed to originate from wake production

and is characterized by flow dynamics governed by the balance between advection and the pressure gradient terms, with turbulent stresses playing a minor role. That is, in the outer layer, the mean momentum balance is given as

$$\bar{U}\frac{\partial \bar{U}}{\partial x} + \bar{W}\frac{\partial \bar{U}}{\partial z} \approx -\frac{\partial \bar{P}}{\partial x}. \tag{6}$$

The turbulent flow is rapidly distorted and a direct proportionality between the hill shape and the flow statistics can be assumed. These assumptions form the basis of the so-called rapid distortion theory (RDT). Spatially, the outer layer is defined for $z - d > h_m$, where h_m is known as the middle-layer depth estimated by solving

$$\frac{h_m}{L} \sim \left[\ln\left(\frac{h_m}{z_o}\right)\right]^{1/2}. \tag{7}$$

The statistics in this layer are expected to scale with the local velocity perturbation $\Delta u/U_b$ as predicted from RDT (given that T_D is the appropriate time scale). In the outer layer, the linearized RDT predicts a reduction in σ_u and a concomitant increase in σ_w, given by (Britter et al. 1981; Belcher and Hunt 1998; Athanassiadou and Castro 2001)

$$\frac{\sigma_u^2(x,z)}{\sigma_{u,b}^2(z)} = 1 - \frac{4}{5}\frac{\Delta u(x,z)}{U_b(z)}, \tag{8}$$

$$\frac{\sigma_w^2(x,z)}{\sigma_{w,b}^2(z)} = 1 + \left(\frac{6}{5} - \frac{2R}{5}\right)\frac{\Delta u(x,z)}{U_b(z)}. \tag{9}$$

Here, $R = \sigma_{u,b}^2/\sigma_{w,b}^2$ which represents the degree of anisotropy existing in the background state ($R = 1$ for an isotropic flow). These reductions and increases occur because the vortex line, and hence the vorticity of the energy-containing eddies (ω_x, ω_y, and ω_z), are distorted by anisotropic straining induced by the mean flow. In particular, over the top of the hill, $\Delta\omega_x \propto \Delta u$ while $\Delta\omega_z \propto (U_b + \Delta u)^{-1}$. Hence, with increasing Δu, $\Delta\omega_x$ increases while $\Delta\omega_z$ decreases. Immediate consequences of the linearized RDT equations is that in the outer layer σ_u and σ_w are in phase with Δu (Belcher and Hunt 1998).

2.4 Inner Layer

As the inner layer is approached, the turbulence effects become significant, modifying the mean momentum balance via

$$\bar{U}\frac{\partial \bar{U}}{\partial x} + \bar{W}\frac{\partial \bar{U}}{\partial z} = -\frac{\partial \bar{P}}{\partial x} - \frac{\partial}{\partial z}\overline{u'w'} - \frac{\partial}{\partial x}\overline{u'u'}. \tag{10}$$

Because $T_D/T_L > 1$ in this layer, the local stretching of large eddies is fast enough to compete with the distortion due to mean flow advection. This layer is called the *local-equilibrium layer* or inner layer because the local eddies relax to equilibrium with the local mean velocity gradient before spatial advection can transport and stretch them. Because of this equilibrium in the inner layer, K-theory can be used to predict *perturbations* in the turbulent stresses or Δu_* even if K-theory may fail to describe the background state. Spatially, the inner layer is defined for $z - d < h_i$, where h_i is known as the inner layer depth estimated by solving

$$\frac{h_i}{L} \simeq \frac{2k_v^2}{\ln(h_i/z_0)}. \tag{11}$$

In this layer, the longitudinal variations of the local statistics are expected to scale with $\Delta u_*^2 = -K_t\,\partial\Delta u/\partial z$.

Using K-theory, the second-order statistics in the inner layer are given by

$$\sigma_u^2 = \frac{1}{3}\sigma^2 - K_t\left(\frac{\partial \bar{U}}{\partial x} + \frac{\partial \bar{W}}{\partial z}\right), \tag{12}$$

$$\sigma_w^2 = \frac{1}{3}\sigma^2 - K_t\left(\frac{\partial \bar{W}}{\partial x} + \frac{\partial \bar{U}}{\partial z}\right), \tag{13}$$

where σ^2 is the total turbulent kinetic energy (TKE). For an incompressible flow, this approximation leads to normalized variances given by

$$\frac{\sigma_u^2(x,z)}{\sigma_{u,b}^2(z)} \approx 1 + \frac{1}{3}\frac{\Delta\sigma^2}{\sigma_{u,b}^2} \tag{14}$$

$$\frac{\sigma_w^2(x,z)}{\sigma_{w,b}^2(z)} \approx 1 + \frac{1}{3}\frac{\Delta\sigma^2}{\sigma_{w,b}^2} - \frac{K_t\partial(\Delta u)/\partial z}{\sigma_{w,b}^2}. \tag{15}$$

Unlike the outer layer scaling, where σ_w^2 increases with increasing Δu, σ_w^2 here tends to decrease with increasing $\partial\Delta u/\partial z$. The so-called middle layer, situated between the inner

and outer regions, is generally assumed to be inviscid but rotational. In this layer, the mean flow undergoes transition from its equilibrium state in the inner layer to being rapidly distorted by advection in the outer layer.

2.5 Canopy Layer

The presence of a canopy sublayer modifies the inner layer arguments in JH75 by, (1) altering the no-slip lower boundary condition, and (2) by introducing the drag term in the mean momentum budget equation so that

$$\bar{U}\frac{\partial \bar{U}}{\partial x} + \bar{W}\frac{\partial \bar{U}}{\partial z} \approx -\frac{\partial \bar{P}}{\partial x} - \frac{\partial}{\partial z}\overline{u'w'} - \frac{\partial}{\partial x}\overline{u'u'} - C_d a \bar{U}^2. \tag{16}$$

Hence, the canopy layer adds two new length scales to the mean momentum balance: L_c and h_c. Here, the second-order statistics (and the velocity component spectra in particular) are complicated by numerous factors (e.g. wake production and short-circuiting of the energy cascade) that prevent an a priori velocity scale from being defined strictly based on mean flow (or shear stress) considerations. In other words, within the canopy layer, $\overline{w'u'}(x, z)$ may no longer be the only leading term for turbulent production because of other mechanisms such as wake production (W_p). Wake production by the mean flow scales as $W_p \sim \overline{U}^3(x, z)/L_c$ (Finnigan 2000; Poggi et al. 2004a; Poggi and Katul 2006, 2008; Cava and Katul 2008), which can exceed the shear production $\overline{w'u'}(x, z)\, d\bar{U}/dz$ in some layers of the canopy even over flat terrain.

One possible consequence of the dominance of W_p inside the canopy is that σ_w^2 (and to a lesser extent σ_u^2) may become in phase with Δu though this phase alignment is not connected with RDT (Poggi and Katul 2008). The rationale for this speculation is due to the fact that the linearized wake production, given by

$$W_{p,l}(x, z) \approx \frac{\bar{U}^3}{L_c} = \frac{U_b^3\,(1 + (\Delta u/U_b))^3}{L_c} \approx \frac{U_b^3}{L_c}\left(1 + 3\,\frac{\Delta u}{U_b}\right) \tag{17}$$

is in phase with Δu (for small $\Delta u/U_b$). On the other hand, shear production, which is the other main source of turbulent energy inside the canopy, scales with $(\partial \Delta u/\partial z)^2$. If wake production becomes the dominant source of turbulent kinetic energy (as may be anticipated for σ_w^2 and to a lesser extent σ_u^2 inside canopies), its action may be to re-align velocity variances to be in phase with Δu in those layers, a mechanism completely absent for a rough bare surface case (Poggi and Katul 2008).

There are two more practical aspects that need to be addressed when dealing with tall-canopy flows over hills: the effect of the canopy on the inner layer depth, and the interplay between the canopy and the hill on the generation of an effective drag at the hill surface. With regards to the first point, it is well established that as z_o increases, h_i gradually increases (roughly, $h_i \sim (L^{0.9}/8)\, z_o^{0.1}$). To illustrate this using a numerical example, consider a cosine hill having a half-length $L = 100$ m and a height $H = 10$ m. Increasing z_o from 0.1 m to 1 m leads to a corresponding increase in h_i from 7.5 m to 12.5 m, though this increase is hardly sufficient to ensure a well-developed inner layer not affected by the canopy sublayer. If $h_c \approx H$ (and $z_o \sim 0.1\, h_c$), then the entire inner layer depth may be immersed within the so-called roughness sublayer often defined as the layer between the ground and $2h_c$ (Raupach and Thom 1981; Finnigan 2000).

With regards to the second point, the total surface force (per unit area per unit fluid density) on the hill is modified from the bare surface case by F_c and given by

$$F_T = F_p + F_\tau + F_c, \tag{18}$$

where F_p, F_τ, and F_c are the pressure force, the surface turbulent shear stress, and the canopy drag force, respectively, given by

$$F_p = \frac{1}{4L}\int_{-2L}^{2L} p(0,x)\frac{\partial z_s}{\partial x}dx, \tag{19}$$

$$F_\tau = \frac{1}{4L}\int_{-2L}^{2L} -\Delta\overline{u'w'}(x,0)dx, \tag{20}$$

$$F_c = \frac{1}{4L}\int_{-2L}^{2L}\left(\int_0^{h_c}\frac{\Delta(u|u|)}{L_c}dz\right)dx. \tag{21}$$

In dense canopies, where $h_c/L_c > 1$, $F_\tau \ll F_c$ and can be neglected. In fact, based on the background state defined here, it is identical to zero. With regards to F_p, the presence of a canopy is likely to complicate the phase relationships between $p(x,0)$ and local topographic gradients. In particular, PK07 have shown that if a recirculation zone on the lee side of the hill in the deeper layers of the canopy occurs, it can modify the pressure field significantly. PK07 reported surface pressure measurements that are asymmetric because of the recirculation zone and require, at minimum, three Fourier modes to describe their overall shape for a train of cosine hills. The implication of this asymmetry on the pressure drag has not been fully explored, except via scaling arguments. These arguments call into question whether an effective roughness length (or drag coefficient) for the combined hill-canopy system is even an appropriate concept. The LES runs chosen here, with one experiment producing recirculation while the other does not, provide a comparative framework to assess the role of recirculation on pressure modulations and concomitant effects on higher-order moments.

2.6 Pressure Variance

Much of the discussion up to this point considers the effects of the hill-canopy system on the velocity variances with no regards to variations in the pressure variance (σ_p^2), perhaps the least understood term in second-order flow statistics. In this section, scaling arguments as to how σ_p is perturbed by the hill are explored. The instantaneous turbulent pressure fluctuation p at a point is given by,

$$\frac{\partial^2 p}{\partial x_i \partial x_i} = -\frac{\partial}{\partial x_i \partial x_j}\left(\underbrace{\left(u_i\bar{U}_j + u_j\bar{U}_i\right)}_{T_1} + \underbrace{\left(u_i u_j - \overline{u_i u_j}\right)}_{T_2}\right), \tag{22}$$

where the first term on the right-hand side is the mean flow-turbulent interaction (hereafter referred to as T_1) and the second term on the right-hand side is the turbulent-turbulent interaction (hereafter referred to as T_2). It is not the intent here to derive a formal equation for σ_p from the above instantaneous equation; rather, it is employed for scaling purposes as follows: by noting that $\partial u_i/\partial x_i = \partial \bar{U}_i/\partial x_i = 0$, the above equation reduces to

$$\frac{\partial^2 p}{\partial x_i \partial x_i} = -2\frac{\partial \bar{U}_i}{\partial x_j}\frac{\partial u_j}{\partial x_i} + \ldots. \tag{23}$$

In a first-order analysis of boundary-layer flow over hills, the largest mean flow gradient is $\partial \bar{U}(x,z)/\partial z$ (i.e. $i = 1$, $j = 3$) and is a logical candidate to be the leading term in T_1. Hence, the instantaneous pressure is given by

$$\frac{\partial^2 p}{\partial x_i \partial x_i} = -2\frac{\partial \bar{U}}{\partial z}\frac{\partial w}{\partial x} + \ldots. \tag{24}$$

To employ Eq. 24 for scaling purposes, it is assumed that the local root-mean-squared amplitudes represent the mean amplitudes of the turbulent fluctuations so that the relevant fluctuations scale as follows: $p \sim \sigma_p$, $w \sim \sigma_w$, and all derivatives have a canonical length scale l (Tennekes and Lumley 1972). When employing such a scaling argument,

$$\frac{\sigma_p}{l^2} \sim 2\frac{\partial \bar{U}}{\partial z}\frac{\sigma_w}{l} + \ldots, \tag{25}$$

and leads to

$$\sigma_p(x,z) \sim 2\,\sigma_w(x,z)\,l(x,z)\,\frac{\partial \bar{U}(x,z)}{\partial z}\ldots. \tag{26}$$

Hence, based on the leading term of the mean-flow turbulent interaction component, σ_p must be in phase with the product of the above three quantities. Because the mixing length is commensurate with the length scales at which $\bar{U}$ changes, it is a natural choice for gradient estimates and results in

$$\sigma_p(x,z) \sim 2\,\sigma_w(x,z)\sqrt{-\overline{u'w'}(x,z)} \tag{27}$$

when $l = l_m$.

In the inner and middle layers, 'in-phase' relationships between σ_p, the turbulent stresses, and σ_w are expected. These scaling arguments, along with how the canopy modifies them, are explored via the LES runs here (subject to the usual subgrid approximations and other LES constraints).

3 The Large-Eddy Simulations (LES)

3.1 Designing the LES Experiments

According to FB04, separation occurs inside the canopy for the layer experiencing an adverse pressure gradient when

$$\frac{Z_s}{h_c} = \frac{1}{2\beta h_c}\ln\left(\frac{U_o^2}{U_h^2}\frac{H}{2}k^2 L_c\right) < 1, \tag{28}$$

where Z_s is the depth at which the onset of separation occurs into the canopy, and U_o is the outer layer velocity. For a hill-canopy set-up with $L = 80\,\mathrm{m}$, $u_* = 0.33\,\mathrm{m\,s^{-1}}$ at the canopy top, $H = 8\,\mathrm{m}$, $h_c = 10\,\mathrm{m}$, $C_d = 0.3$, and $\beta = 0.33$ results in $Z_s/h_c > 1$ for 10 rods m^{-2} and $Z_s/h_c < 1$ for 100 rods m^{-2} (see Fig. 2). Hence, based on FB04, it is anticipated that when $a = 10$ rods m^{-2}, no recirculation occurs, and conversely when $a = 100$ rods m^{-2}.

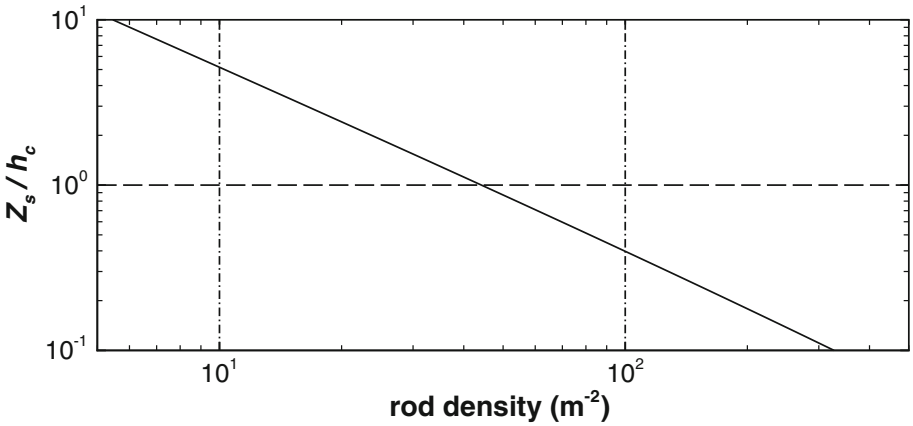

Fig. 2 The variation of the FB04 computed depth (*solid line*) at which the onset of separation occurs into the canopy (Z_s) normalized by the canopy height (h_c) as a function of the rod density (a). If $Z_s/h_c > 1$, no separation occurs. The two *dash-dot vertical lines* represent the rod densities chosen for the LES runs. For reference, the $Z_s/h_c = 1$ is shown (*dashed horizontal line*)

These are the two rod densities chosen for the LES runs here. Although not significant for the analysis presented, it is useful to note that the sparse (non-separating) case falls outside the regime of validity for FB04's analytic theory (Fig. 3). Moreover, the dense canopy (separating) case falls in a regime in which the pressure is non-interactive (or fixed)—and the vertical-velocity-induced perturbations by the hill are insufficient to significantly modify the outer-layer pressure field (as assumed in FB04).

3.2 Numerical Implementation

The fundamental details of the LES code utilized in these two experiments have been previously documented (Sullivan et al. 2008) and its capability to reproduce turbulent flow over rough hills was previously demonstrated through a comparison with wind-tunnel measurements (Patton et al. 2006). Therefore, only a basic description of the LES and modifications made to the code are discussed here. The LES solves a set of filtered, unsteady, three-dimensional, incompressible Boussinesq equations. A conformal mapping is utilized to transform the grid from the physical domain into a Cartesian computational domain. Subfilter-scale momentum fluxes that arise from the filtering are parameterized using a simple eddy viscosity model following Deardorff's turbulence kinetic energy formulation (Deardorff 1980). Buoyancy and Coriolis forces are neglected. A mixed finite-difference pseudo-spectral scheme is employed to calculate derivatives, and to avoid aliasing errors, the top one-third wavenumbers are explicitly filtered in the x and y directions. Hence, the characteristic length scale defining the separation between the resolved- and subfilter-scale motions is $\Delta f = (\frac{3}{2}\Delta_x \times \frac{3}{2}\Delta_y \times \Delta_z)^{1/3}$. Periodic boundary conditions are used in the horizontal directions (x and y), and in the vertical direction (z) the upper boundary is specified as a frictionless rigid lid, and the bottom boundary assumes a drag-law formulation from the first grid point down to the ground with $z_o = 1 \times 10^{-4}$ m. The flow is driven by a specified longitudinal pressure gradient equal to 1.13×10^{-5} m s^{-2}.

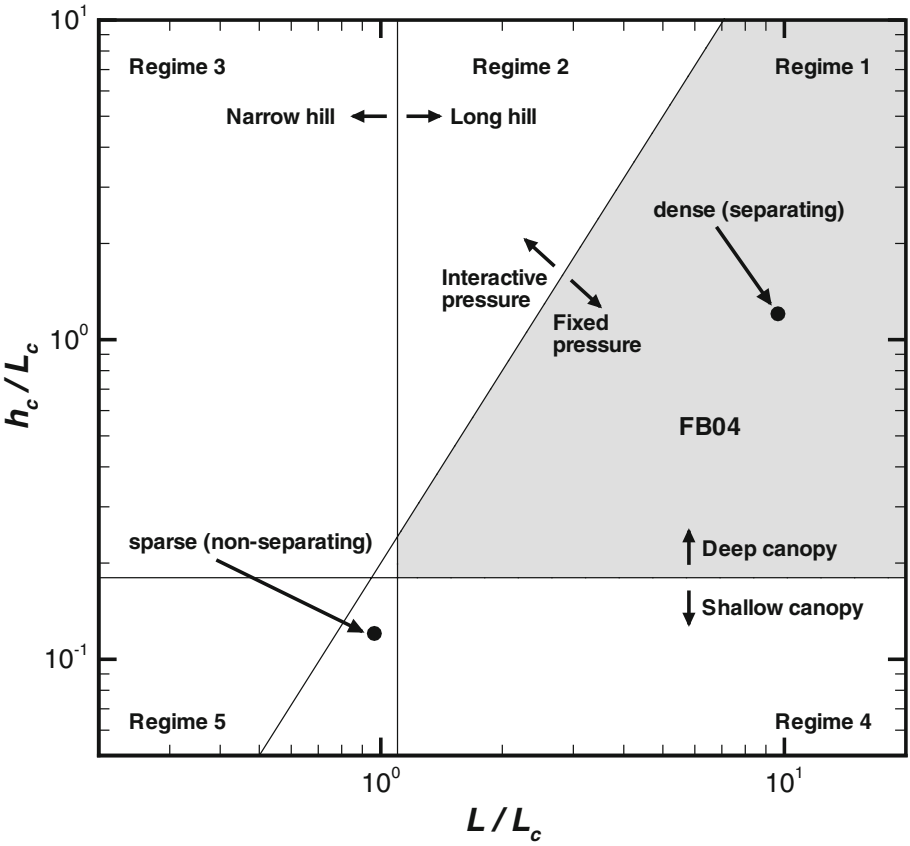

Fig. 3 Length scale regimes imposed by hill geometry and canopy morphology classifying hills as narrow or long, and the canopies as deep or shallow (following Poggi et al. 2008). The envelope $h_c/L_c = 2(H/L)(L/L_c)^2$ delineates regions in which the mean vertical velocity inside the canopy is expected to be large enough to affect the outer-layer pressure; flow regimes above this envelope are referred to as 'interactive' pressure regimes, and flow regimes below this envelope are referred to as 'fixed' pressure regimes. Finnigan and Belcher's (2004) analytic theory is valid in the shaded area (Regime 1). The cases discussed here are marked and can be classified as residing in Regime 5 for the sparse (non-separating) case and in Regime 1 for the dense (separating) case

The undulating bottom boundary, $f(x)$, does not vary laterally or in time, and is specified as:

$$f(x) = \frac{H}{2} \cos\left(\frac{\pi x}{2L} + \pi\right), \tag{29}$$

which is a function of horizontal location x (see Table 1). The domain is 640 m×320 m×256 m resolved by 640 × 320 × 128 grid points (in the N_x, N_y, and N_z directions). In the computational space, the horizontal spacing is 1 m for all x and y directions and a constant vertical spacing (= 0.5 m) is used for the first twenty grid points resolving the canopy. Above the canopy, algebraic grid stretching with a factor of 1.02 is used to resolve the rest of the vertical domain. In the physical domain, the canopy is resolved by 16 to 24 grid points because the horizontal grid lines follow the terrain and are more tightly spaced at the top of the hills than at the bottom. Towards the bottom of the domain, the vertical grid lines in the physical

Table 1 Hill properties, canopy attributes, and canonical length scales for the two LES runs

	No separation	With separation
Hill properties		
Hill shape	$f(x) = \frac{H}{2}\cos\left(\frac{\pi x}{2L} + \pi\right)$	
Half length (L), [m]	80	80
Height (H), [m]	8	8
Canopy properties (rods)		
Number of rods per unit area (n_r), [m^{-2}]	10	100
Rod diameter (d_r), [m]	0.004	0.004
Rod height (h_c), [m]	10	10
Frontal area index ($a = n_r \times d_r$), [m^{-1}]	0.04	0.4
Canopy drag coefficient (C_d)	0.3	0.3
Porosity ($n_p = 1 - (\pi/4)\, a\, d_r$)	$\sim$1	0.999
Mean momentum absorption (β)	0.25	0.40
Computed length scales (m)		
Middle-layer depth (h_m)	30	47
Inner-layer depth (h_i)	10	15
Adjustment length (L_c)	83	8.3
Zero-plane displacement (d)	3.5	7.3
Aerodynamic roughness length (z_o)	0.7	2.7
Separation depth (Z_s)	30 ($>h_c$)	3.2 ($<h_c$)

domain also curve so that they are perpendicular to the horizontal grid lines and the hill surface.

Explicit filtering of the Boussinesq equations in the presence of vegetation produces terms in the equations representing both the viscous and pressure drag imparted by the vegetation on the flow (Raupach and Shaw 1982; Finnigan and Shaw 2008). Here, the term representing the viscous drag is neglected based upon a scale analysis of the relative importance of the pressure drag to the viscous drag (Shaw and Patton 2003), and the pressure drag imparted by the canopy is parameterized as a three-dimensional unsteady drag law formulation, e.g.:

$$F_{d,i}(x, y, z, t) = |U(x, y, z, t)| u_i(x, y, z, t)/L_c, \tag{30}$$

where u_i is the instantaneous local wind velocity and |U| is the local scalar wind speed. In the physical domain, the canopy density distribution is constant vertically. It is assumed that the work performed by the canopy drag force converts energy from the resolved-scale flow to subfilter-scale kinetic energy at a scale small enough that it is immediately dissipated to heat. On the other hand, all wake-generated motions larger than Δf are explicitly resolved (Dwyer et al. 1997; Shaw and Patton 2003). Table 1 provides all the relevant length scales for each simulation.

4 Results and Discussion

The bulk flow statistics and the background states computed from the LES are discussed first followed by an analysis of how the phase relationships are affected by the presence or absence of a recirculation zone inside the canopy. In particular, the phase relationships to be studied include whether $\sigma_u^2(x,z)/\sigma_{u,b}^2(z)$ and $\sigma_w^2(x,z)/\sigma_{w,b}^2(z)$ remain in phase with Δu in the outer layer and with the local turbulent stresses in the inner layer. Next, the impact of canopy density variations on these phase relationships through wake production is explored in two regions of the canopy: upper and lower. The upper canopy layer may still be affected by inner-layer dynamics (in FB04 this impact was 'communicated' via a matching function), while the lower canopy layer is less likely to be affected by the inner-layer dynamics.

The phase relationship between $\sigma_p(x,z)/\sigma_{p,b}(z)$ and Δu or $\partial\Delta u(x,z)/\partial z$, rarely evaluated in analytical models or experiments, is also explored across the various layers above the hill surface. Finally, canopy-induced modifications to F_p and F_c and thus the effective drag parameterizations will be discussed in light of cases with separation versus no separation.

4.1 Mean Flow Properties

Figure 4 compares the LES derived spatial variation of the first and second moments of the flow field for the non-separating and separating cases. In agreement with predictions by FB04 (see Fig. 2), the LES results for the mean flow confirm the absence of a layer of reversed flow for $a = 10\,\text{rods m}^{-2}$ and the presence of a layer of reversed flow for $a = 100\,\text{rods m}^{-2}$ (depicted by the pink region within the canopy in the lee of the hill in the upper right panel of Fig. 4). For the non-separating case, the spatial patterns in mean velocity and turbulent stress also follow predictions from FB04. Inside the canopy, the mean velocity increases for upwind conditions up to the hill summit and then decreases on the lee-side face. The magnitude of the turbulent stresses is reduced (less negative) at the upwind side but is increased (in magnitude) on the lee side.

Near the canopy top and just above the canopy (within the inner layer), there is a zone of intense turbulent stresses on the lee side of the hill, and conversely on the upwind side. These intense shear zones appear to advect longitudinally, diffusing upward into the middle layer (more so for the separating case), but partially dissipated in the outer layer for $z \sim L$ (as expected from RDT).

The spatial patterns are qualitatively similar for σ_u and σ_w already hinting that they are approximately in phase with turbulent stresses in the inner and canopy layers (for the non-separating case). Also evident from Fig. 4 is the fact that the intense σ_u zones originating in the inner layer are dissipated faster as the middle layer is approached when compared to σ_w, qualitatively consistent with RDT predictions for the middle layer, though the precise phase relationships are not (as we show later).

4.2 Background States

The profiles of the background states are presented in Fig. 5. These profiles are consistent with expectations from 'flat-world' canopy flows and other studies (Besio et al. 2001). The normalized mean velocity increases inside the canopy with increasing height near-exponentially and then near-logarithmically above the canopy thereafter. The LES computed mean

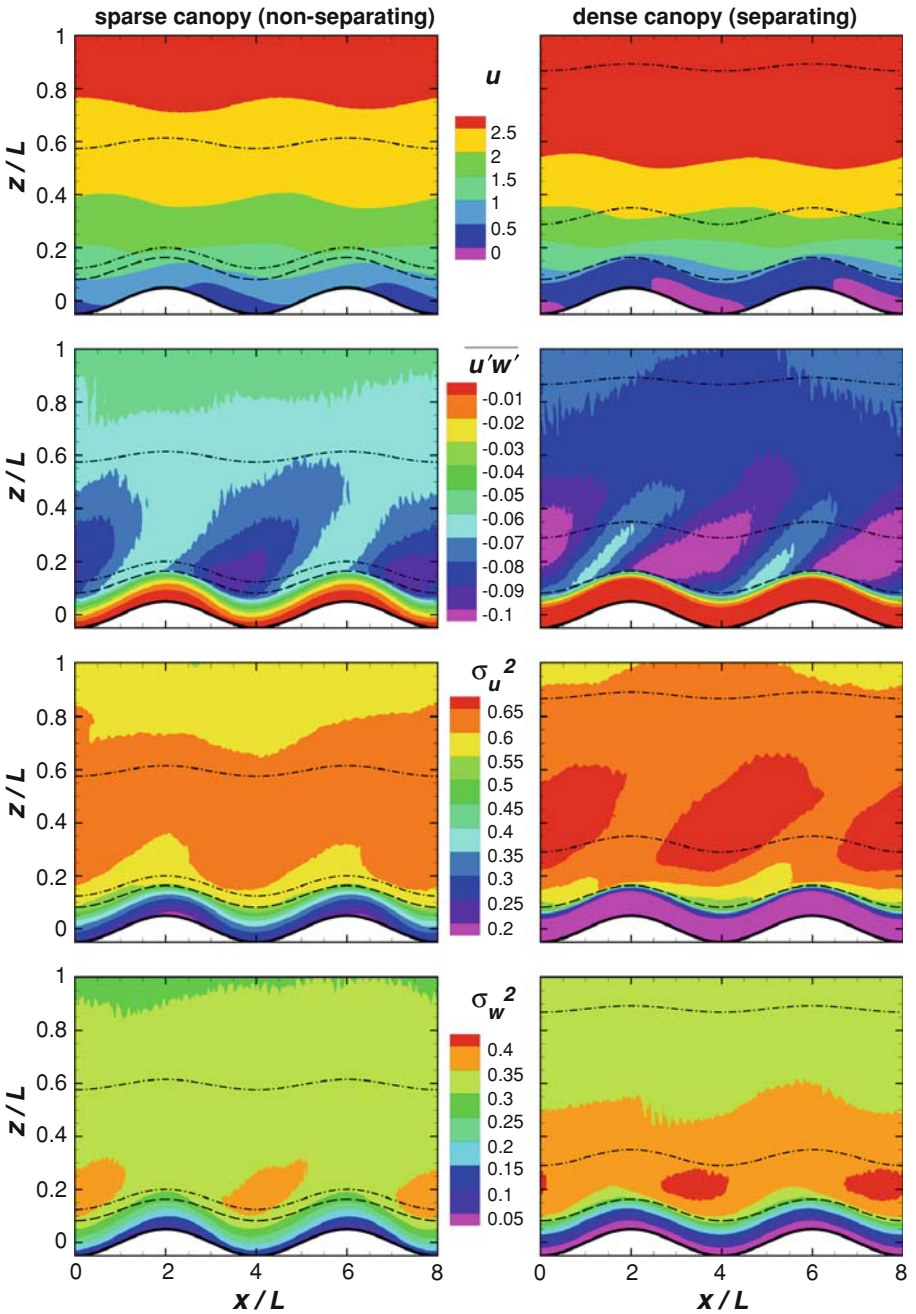

Fig. 4 The spatial variation of the first and second moments of the flow statistics for the non-separating (*left panels*) and separating (*right panels*) cases, respectively. The panels, from *top to bottom*, are: mean velocity ($\mathrm{m\,s^{-1}}$), turbulent shear stress ($\mathrm{m^2\ s^{-2}}$), longitudinal velocity standard deviation ($\mathrm{m\,s^{-1}}$), and vertical velocity standard deviation ($\mathrm{m\,s^{-1}}$). Starting from the lowest line, the *dashed lines* indicate the canopy top, inner layer, and middle layer respectively. The mean flow direction is from left to right

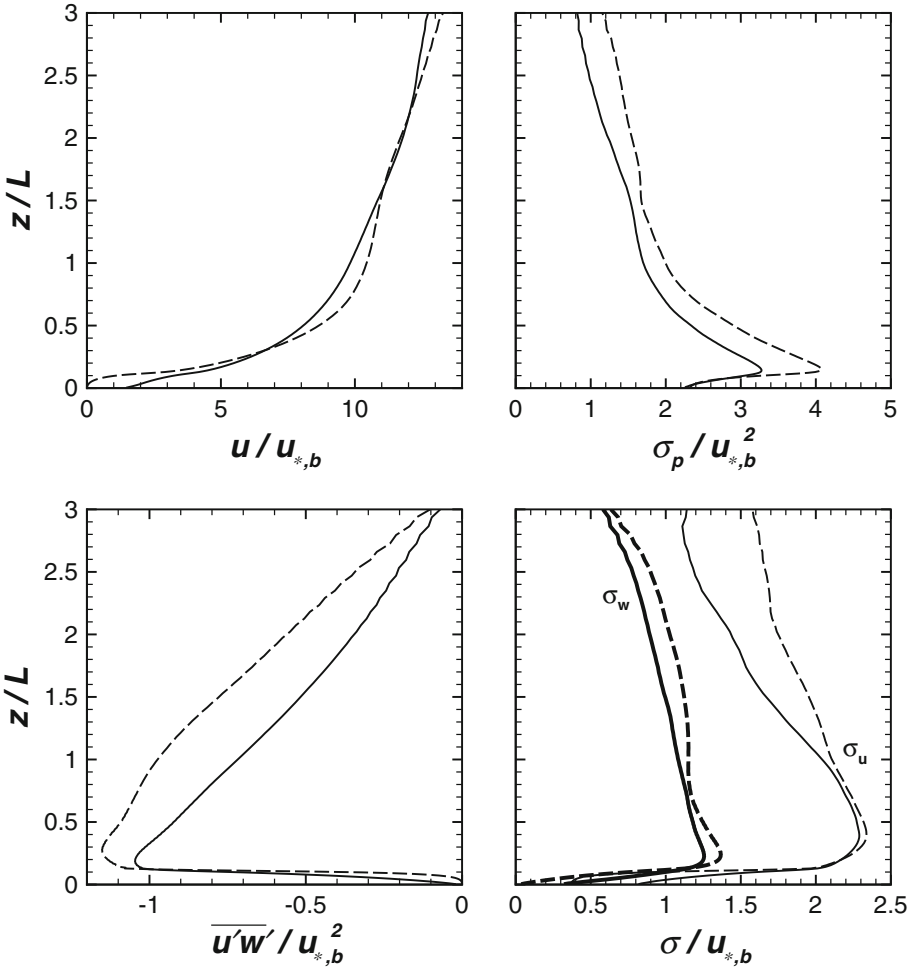

Fig. 5 The vertical variation of the longitudinally-averaged mean velocity (*top left*), turbulent static pressure standard deviation (*top right*), turbulent shear stress (*bottom left*), and the two component velocity standard deviation (*bottom right*). *Solid lines* are for the non-separating case while *dashed lines* are for the separating case. The normalizing velocity variable is u_* and normalizing length is the hill half-length L

momentum absorption at the canopy top were about 0.3 and 0.4 for the non-separating and separating cases, respectively. These values are not too different from the 0.33 reported for dense canopies on flat terrain (Raupach 1994; Raupach et al. 1996; Massman 1997; Poggi et al. 2004b).

The background turbulent shear stress rapidly decays inside the canopy because of momentum absorption, but is approximately linear for much of the inner and middle regions. Using regression analysis, it was confirmed that the linear increase in background turbulent shear stress is the same for the separating and non-separating cases (as expected, given that the two LES runs are forced by the same mean pressure gradient). Note from Fig. 5 that the peak magnitude of the background shear stress for the separating run is displaced upwards just above the canopy; this shift and increase are likely induced by some asymmetry in $P(x, z)$ and $\overline{u'w'}(x, z)$ produced by the hill-canopy system.

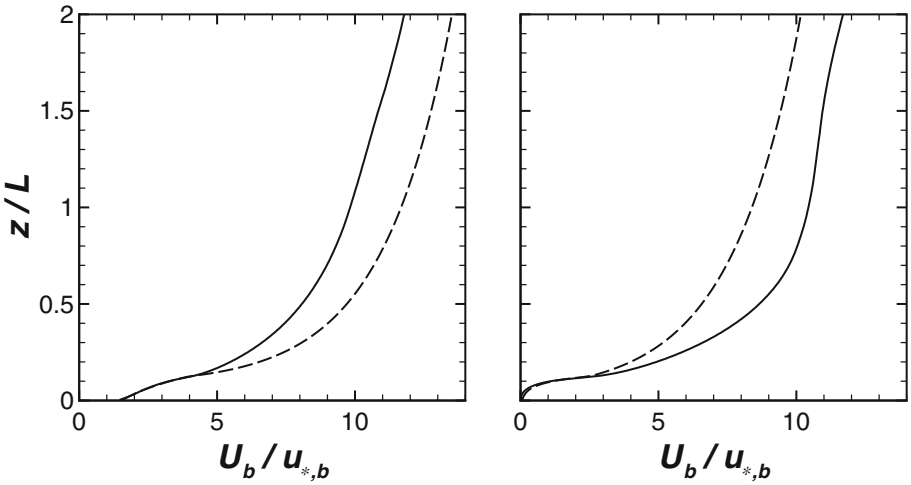

Fig. 6 Comparisons between the longitudinally-averaged mean velocity from the LES (*solid line*) and the background velocity from the flat-terrain formulation (*dashed line*) for the non-separating (*left*) and separating (*right*) cases

The normalized root-mean-squared velocity components are attenuated inside the canopy with decreasing z as expected for 'flat-world' canopy flows, and their peak values near the canopy top are comparable to what was generally reported for a near-neutral atmospheric surface layer (ASL) (i.e. $\sigma_u/u_* \approx 2.3$, and $\sigma_w/u_* \approx 1.25$). Canopy density variations do not significantly affect these values near the canopy top.

Likewise, for the non-separating case, the normalized root-mean-squared static pressure fluctuations near the canopy top $\sigma_p/u_*^2 \approx 3.3$ is surprisingly similar to that reported for near-neutral ASL flows (Katul et al. 1996). This value falls to about $\sigma_p/u_*^2 \approx 2.2$ deep inside the canopy, which is consistent with ground pressure measurements reported elsewhere for a hardwood canopy (Katul et al. 1996). For the separating case, $\sigma_p/u_*^2 \approx 4.1$, which is significantly higher than the non-separating case. This finding is consistent with Eq. 27 and the zones of intense shear reported in Fig. 4 for the case with the denser canopy (noting that σ_w did not appreciably change with leaf area density above the canopy).

Upon regressing background σ_p/u_*^2 on background $\overline{u'w'}/u_*^2$ for the above-canopy layers, the regression slopes are -2.2 and -2.3 and coefficients of determination (r^2) were 0.70 and 0.88 for the non-separating and separating cases, respectively. Again, the near-equality in these regression slopes is consistent with Eq. 27 given that the background σ_w/u_* profile does not vary appreciably with leaf area density above the canopy.

The U_b determined from Eq. 2 are also compared to the longitudinally-averaged LES velocity in Fig. 6. Inside the canopy, good agreement is noted between LES computed and modelled U_b when using a constant l, but above the canopy, the two results diverge. Equation 2 overestimates the background velocity for the non-separating case and underestimates the background velocity for the separating case. Because of these disagreements, the background state determined from longitudinal averaging of the LES results is used throughout to define the hill-induced perturbations in the flow statistics.

These disagreements are connected with the non-linear vertical variation in the mixing lengths (not shown). Moreover, when computing the vertical mixing length inside the canopy for the two LES runs, the values are not constant. A layer of enhanced mixing length is evident in the lower canopy layers followed by a layer of reduced mixing length in the upper canopy

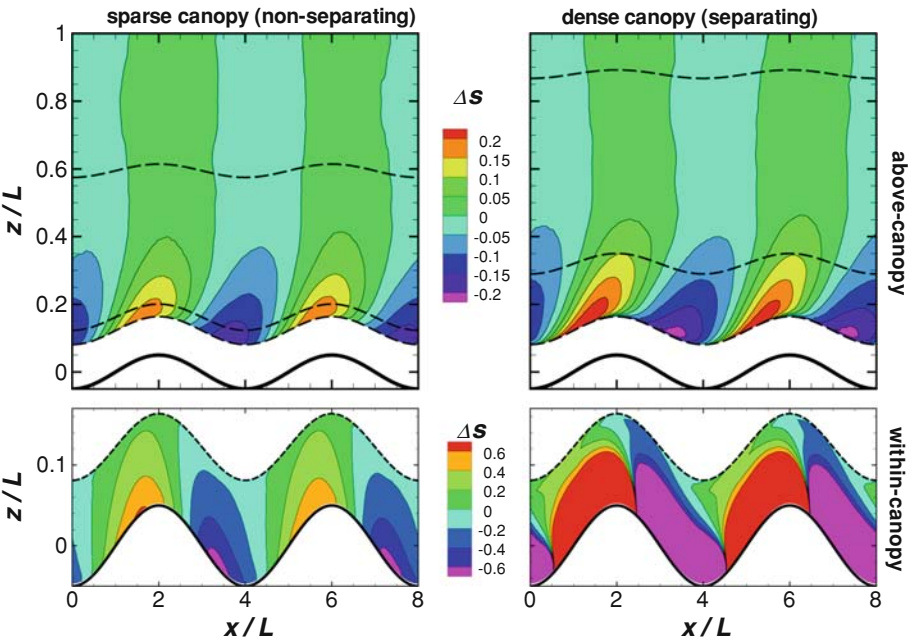

Fig. 7 The spatial variation of the over-speeding ratio above the canopy for the non-separating (*left*) and the separating (*right*) cases. The *dashed lines* indicate the canopy top, the inner layer and middle layer depths. The vertical (z) and longitudinal (x) distances are normalized by the hill half-length (L)

layers, consistent with LES results reported elsewhere (Ross 2008) and flume experiments (PK07). However, the agreement between LES and modelled background velocity appears robust to this variation in mixing length inside the canopy.

4.3 Over-speeding Ratio

Using the LES computed U, the over-speeding ratio above the canopy, given by

$$\Delta S(x,z) = \frac{U(x,z) - U_b(z)}{U_b(z)}, \tag{31}$$

is presented in Fig. 7, with $U_b(z)$ given from the LES results in Fig. 5. Naturally, the highest and lowest over-speeding ratios are inside the canopy. FB04 demonstrated that, due to the presence of a canopy, the maximum over-speeding location is near the summit but is shifted upwards from $h_i/3$ to h_i and appears reduced by some 20% when compared to flow over a bare-surface hill with equal z_o. For the LES case presented here, the maximum $\Delta S = 0.18$ occurs near the top of the inner layer consistent with FB04. A number of laboratory measurements have reported a higher $\Delta S = 0.28 \rightarrow 0.30$ for flows over an isolated hill and train of hills without tall canopies (Britter et al. 1981; Athanassiadou and Castro 2001). However, it is important to note that this difference in maximum ΔS cannot be divorced from the definition of U_b adopted here (vis-à-vis the isolated hill cases).

Further inspection of Figs. 4 and 7 suggests that variations in ΔS are correlated with shear-stress variations. In fact, for $h_c < z < h_m$, when regressing ΔS upon $\Delta\overline{u'w'}(z,x)$,

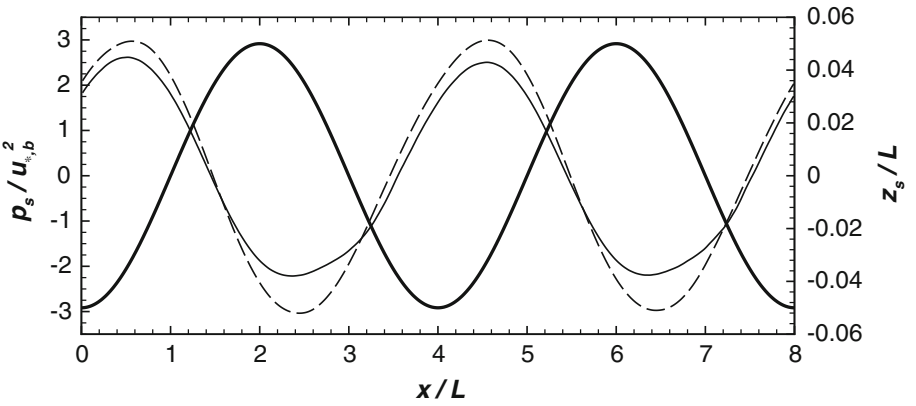

Fig. 8 The variation of the normalized mean surface pressure ($p_s/u_{*,b}^2$) along the hill surface for the non-separating (*thin solid line*) and separating (*thin dashed line*) cases. The normalized hill shape function (z_s/L) is also shown (*heavy solid line*) to illustrate phase relationships between topographic variations and the mean ground pressure. The longitudinal distance (x) and hill-shape function (z_s) are normalized by the hill half-length (L) and the mean surface pressure is normalized by the squared background friction velocity ($u_{*,b}$)

a significant proportion (∼70%) of the variability in $\Delta S(x, z)$ is explained by variations in $\Delta\overline{u'w'}(z, x)$, as expected in the inner layer.

4.4 Mean Pressure Perturbations

For the two LES cases, pressure perturbations are well correlated with topography but not precisely out-of-phase with topography (Fig. 8). This finding is in agreement with closure modelling in RV05 and detailed measurements in PK07, where the minimum pressure perturbation was shifted beyond the hill summit. For the separating case, this shift increases up to $L/2$. However, as anticipated from Fig. 3, the recirculation zone and vertical velocity excursions are not expected to dramatically affect pressure perturbations in the outer layer, and this explains why the pressure remains approximately (but not precisely) out-of-phase with the topography.

The importance of these minor shifts to the overall drag on the hill is considered next. The calculations discussed here suggest that the overall drag on the hill surface is dominated by F_p, which is at least one order of magnitude larger than the canopy drag contribution (or ground shear stress). The values of $F_p/u_{*,b}^2$ are 5.2 and 6.2, respectively for the non-separating and separating LES cases. Hence, the effects of mean re-circulation and concomitant shifts in the location of the minimum pressure with respect to the hill summit enhanced the pressure drag by 15% above the non-separating case. This is not a minor adjustment given that the LES runs were identical in all respects except for the number of rods.

4.5 Velocity Perturbations

Figure 9 presents the hill-induced spatial variation of the normalized mean velocity, $\Delta u(x, z)/u_*$, turbulent stresses, $\Delta\overline{u'w'}/u_*^2$, and velocity variances, $\Delta\sigma_u^2(x, z)/\sigma_{u,b}^2(z)$ and $\Delta\sigma_w^2(x, z)/\sigma_{w,b}^2(z)$. For a closer inspection of the phase relationships, four reference levels are considered and shown in this figure. In the outer layer, the reference level is selected as $z = h_m + d$; for the inner layer, the reference level is set to $z = d + h_i/2$; for the upper

canopy layer, the reference level is set to $z = 0.8\,h_c$; and for the lower canopy layer, the reference level is set to $z = 0.2\,h_c$.

4.5.1 Outer-Layer Scaling

Figure 10 shows the longitudinal variations of $\Delta u(x,z)/U_b(z)$, $\sigma_u^2(x,z)/\sigma_{u,b}^2(z)$, $\sigma_w^2(x,z)/\sigma_{w,b}^2(z)$ at the outer-layer reference level along with RDT predictions for the isotropic case ($R = 1$). The calculations were repeated for the anisotropic case with R defined using the anisotropy ratio of the background state (not shown). We find that the isotropic state better captures the amplitude variability range, and this scenario is adopted in the subsequent discussion. From this figure, the maximum $\Delta u(x,z)/U_b(z)$ is nearly in phase with topography, though the minimum values are not. Lagged correlation analysis between $\Delta u(x,z)/U_b(z)$, $\sigma_u^2(x,z)/\sigma_{u,b}^2(z)$ and $\sigma_w^2(x,z)/\sigma_{w,b}^2(z)$ demonstrated that $\Delta u(x,z)/U_b(z)$ explains much of the variation in the normalized variances with maximum lagged correlation coefficient $r = 0.8$ for the non-separating case, but lower correlations for the separating case are noted with $|r| < 0.6$. Given the similarities in the upper boundary conditions across the two runs, this difference between the two runs suggests that the middle-to-outer layer flow field is partially affected by the canopy. Moreover, the phase relationships for both runs are not correctly predicted by RDT.

Cross-correlation analysis clearly shows how the canopy density affects the phase relationships. For the non-separating case, the phase differences between $\sigma_u^2(x,z)/\sigma_{u,b}^2$ and $\sigma_w^2(x,z)/\sigma_{w,b}^2(z)$ with $\Delta u(x,z)/U_b(z)$ were small. However, these phase relationships are more distorted with increasing canopy density.

Figure 9 offers more hints as to why RDT may not fully explain the phase relationships between $\Delta u(x,z)/U_b(z)$, $\sigma_u^2(x,z)/\sigma_{u,b}^2(z)$ and $\sigma_w^2(x,z)/\sigma_{w,b}^2(z)$. The shear-stress perturbations (and their vertical gradients) are not entirely 'dissipated' above h_m and they retain some coherent longitudinal structure. Hence, the momentum balance in the middle to outer layer may be 'contaminated' by $\partial\overline{u'w'}/\partial z$. One plausible explanation is that this 'contamination' may originate from the imposed upper boundary condition on the LES, but this upper boundary condition was the same for both LES experiments, and its effects are to induce a 'de-correlation' between u' and w' (frictionless lid).

Lagged correlation analysis between $\Delta u(x,z)/U_b(z)$ and $\sigma_p(x,z)$ demonstrates that $\Delta u(x,z)/U_b(z)$ can explain much of the longitudinal variation in the turbulent pressure (maximum $r = 0.9$) for the non-separating case. For the separating case, this maximum correlation remains significant but substantially lower than 0.9. Moreover, $\sigma_p(x,z)$ lags behind $\Delta u(x,z)/U_b(z)$. The lagged correlation analysis between $\Delta u(x,z)/U_b(z)$ and $\sigma_p(x,z)$ is similar to that of $\Delta u(x,z)/U_b(z)$ and $\sigma_u^2(x,z)/\sigma_{u,b}^2(z)$ in terms of phase relationships—again suggestive that the longitudinally unconstrained larger-scale eddies affect both pressure and longitudinal velocity across the hill in a similar way. This finding is consistent with the inactive eddy hypothesis and low-frequency spectral similarity laws between u and p reported by others (Katul et al. 1996) given that these eddies do not transport much momentum in this part of the boundary layer.

4.5.2 Inner-Layer Scaling

Figure 11 shows the longitudinal variations of $\Delta uw(x,z)/\overline{u'w'}_b(z)$, $\sigma_u^2(x,z)/\sigma_{u,b}^2(z)$, and $\sigma_w^2(x,z)/\sigma_{w,b}^2(z)$ at the inner-layer reference level. The longitudinal variations of both variances are well explained by $\Delta uw(x,z)/\overline{u'w'}_b(z)$ (maximum $\rho > 0.8$) as expected from

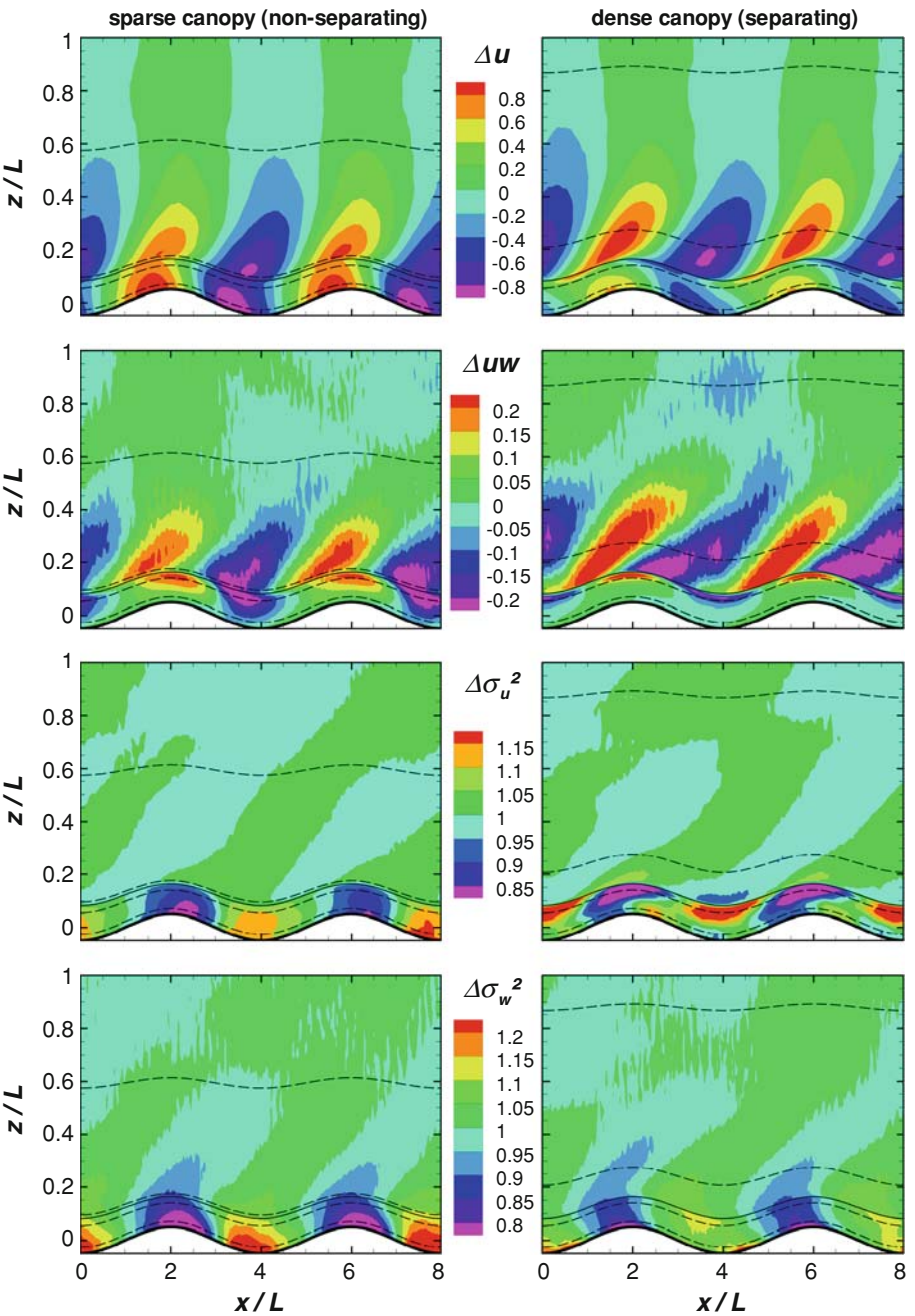

Fig. 9 Same as in Fig. 4 but for the hill-induced perturbations, i.e. deviations from the background. The *dashed lines* are levels for which phase relationships are to be presented

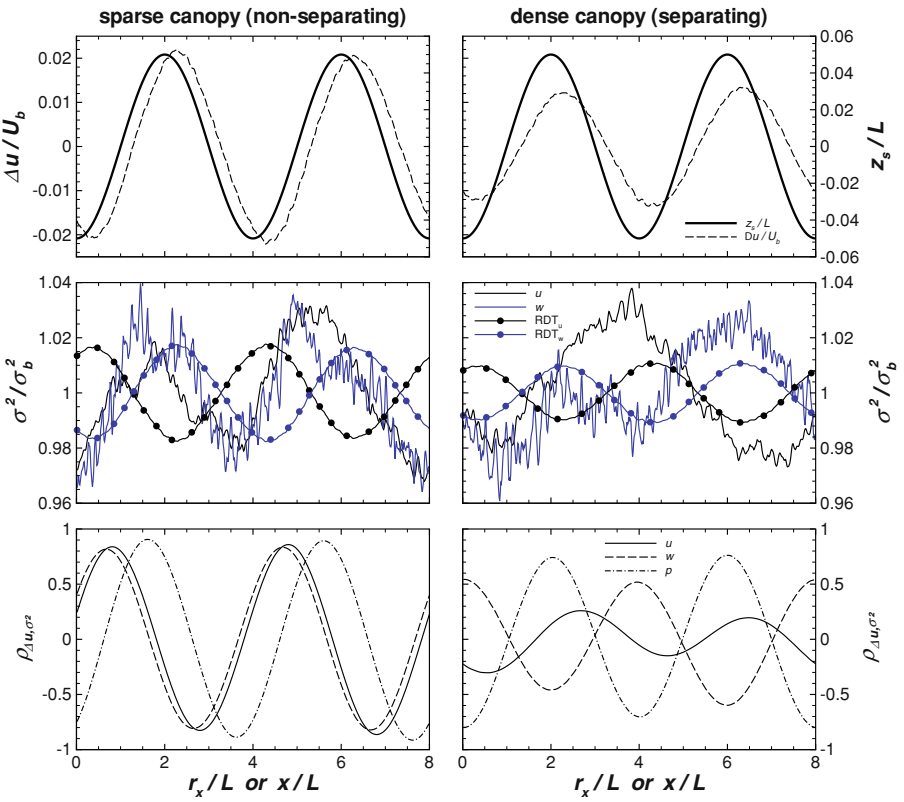

Fig. 10 Phase relationships between second-order statistics and normalized $\Delta u/U_b$ above the middle layer for the non-separating (*left*) and the separating (*right*) cases. *The panels from top to bottom* present: the longitudinal variation of normalized Δu (*dashed line*) and the hill surface (*solid line*) (*top panels*); the variation of the LES-derived longitudinal (*black line*) and vertical (*blue line*) velocity component variances normalized by the background state, along with predictions from RDT for $R = 1$ for the longitudinal (*black dot line*) and vertical (*blue dot line*) velocity variances (*middle panels*); and, the cross-correlation between Δu and the velocity variances for the longitudinal (*solid black*), vertical (*dashed*) components, and the pressure variance (*dash-dot, lower panels*). The normalizing variable for the lagged cross-correlation (r_x) and longitudinal (x) distances is L

inner-layer scaling. In fact, longitudinal variations in $\sigma_w^2(x,z)/\sigma_{w,b}^2(z)$ are almost perfectly correlated with $\Delta uw(x,z)/\overline{u'w'}_b(z)$ for both experiments. In the non-separating case, the maximum negative correlation between $\Delta uw(x,z)/\overline{u'w'}_b(z)$ and $\sigma_w^2(x,z)/\sigma_{w,b}^2(z)$ is shifted slightly upwind of the hill crest with $\sigma_u^2(x,z)/\sigma_{u,b}^2(z)$ shifted nearly an equal amount downwind of the crest. This is in contrast to the separating case where $\Delta uw(x,z)/\overline{u'w'}_b(z)$ and $\sigma_w^2(x,z)/\sigma_{w,b}^2(z)$ are almost perfectly anti-correlated with each other at the hill crest.

Recall that K-theory predicts that $\sigma_w^2(x,z)/\sigma_{w,b}^2(z)$ is affected by $K_t\,(\partial\Delta u/\partial z)$, which is absent from the $\sigma_u^2(x,z)/\sigma_{u,b}^2(z)$ expression (compare Eqs. 14, 15). Hence, this term primarily increases the maximum correlation coefficient between $\sigma_w^2(x,z)/\sigma_{w,b}^2(z)$ and $\Delta uw(x,z)/\overline{u'w'}_b(z)$ and further aligns them together thereby enhancing their in-phase relationships (compared to $\sigma_u^2(x,z)/\sigma_{u,b}^2(z)$).

With regards to the lagged correlation analysis between $\Delta uw(x,z)/\overline{u'w'}_b(z)$ and σ_p, the outcome is almost the same as for $\sigma_u^2(x,z)/\sigma_{u,b}^2(z)$, which is similar to the outer-layer finding

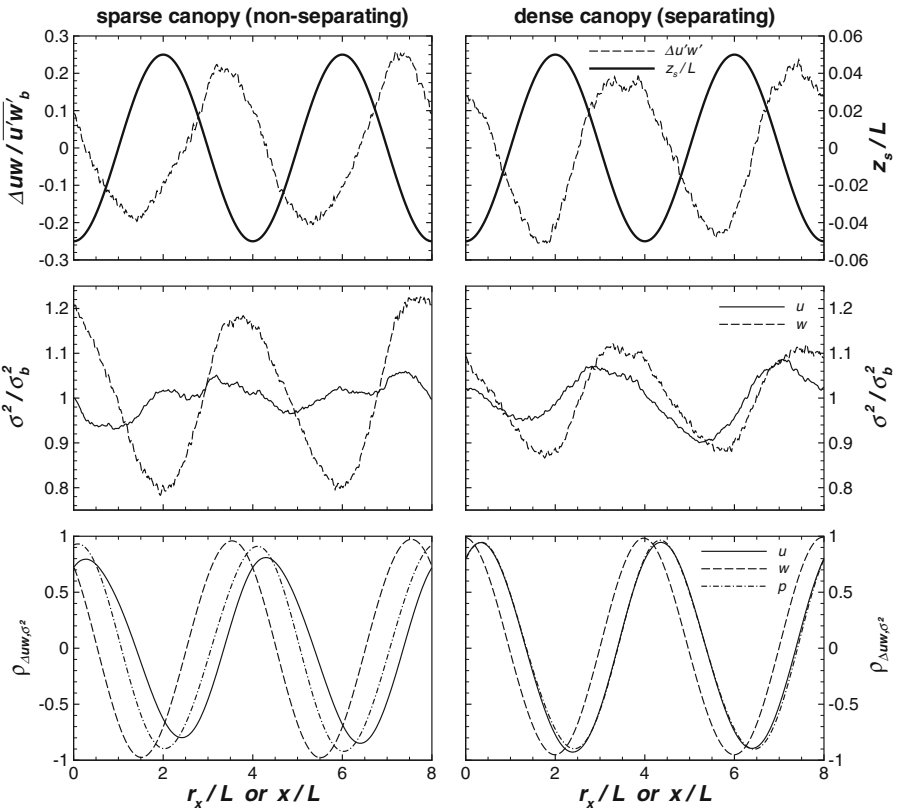

Fig. 11 Same as in Fig. 10 with two changes: (1) this figure presents Δuw instead of Δu, and (2) this figure depicts results for the inner layer instead of the middle layer

in Fig. 10, that σ_p and $\sigma_u^2(x, z)/\sigma_{u,b}^2(z)$ are largely in phase. In short, the phase analysis here is clearly suggestive that the hill-induced vertical velocity standard deviation fluctuations do scale with the local shear stress in the inner-layer, consistent with the flume experiments in PK07. In the PK07 experiments, the within-canopy and inner-layer profiles collapsed reasonably well when the vertical velocity was normalized with the local u_*. Whether for the LES or the flume experiments, this collapse is suggestive that the so-called moving equilibrium hypothesis (Yaglom 1979) may be applicable to modelling σ_w from u_*. This hypothesis argues that if u_* varies slowly in the plane parallel to the surface, then u_* can be considered as a local velocity scale (for inner-layer scaling here), and the forest-hill system can be decomposed into quasi-homogeneous patches with each patch characterized by its own local velocity. The implications of this hypothesis to modelling scalar dispersion on gentle hills covered with a canopy cannot be over-stated given that these models generally require σ_w as input.

On the other hand, both the LES and the flume experiments demonstrate that variability in σ_u is not entirely explained by variability in u_*. One plausible explanation, consistent with the earlier findings here about the phase relationships in the outer layer, is that σ_u is affected by inactive eddies whose length scale permits them to sample a larger portion of the topographic disturbances. Since these eddies do not contribute much to the local shear

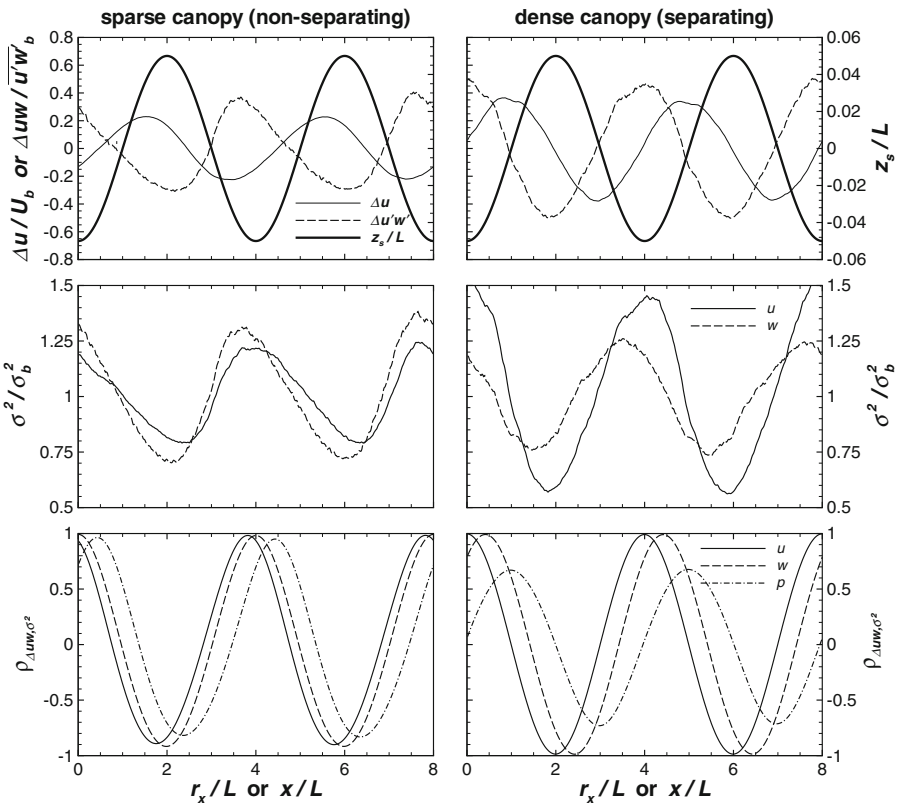

Fig. 12 Same as in Fig. 10 but for Δuw (*solid thin line, top panel*) instead of Δu (also shown as a *dotted line, top panel*) and for the upper canopy instead of the middle layer. The Δu variations are included here because they are in phase with the wake production

stress, some de-coupling between σ_u and u_* variations occurs and u_* no longer becomes the appropriate local velocity (as stipulated by the moving equilibrium hypothesis).

4.5.3 Upper Canopy Layer Scaling

Figure 12 shows the longitudinal variations of $\Delta u(x,z)/U_b(z)$ (thin dashed line, top panel), $\Delta uw(x,z)/\overline{u'w'}_b(z)$ (thin solid line, top panel), $\sigma_u^2(x,z)/\sigma_{u,b}^2(z)$ (thin solid line, middle panel), and $\sigma_w^2(x,z)/\sigma_{w,b}^2(z)$ (thin dashed line, middle panel) at the upper canopy layer reference level. For the non-separating case, $\Delta uw(x,z)/\overline{u'w'}_b(z)$, $\sigma_u^2(x,z)/\sigma_{u,b}^2(z)$ and $\sigma_w^2(x,z)/\sigma_{w,b}^2(z)$ are almost in phase, and the shear-stress perturbations explain almost 100% of the longitudinal variability in the variances.

For the separating case, wake production P_{wake} is expected to become significant in the upper canopy (not shown here). The influence of P_{wake} appears minor on $\sigma_u^2(x,z)/\sigma_{u,b}^2(z)$, which remains primarily in phase with $\Delta\overline{u'w'}$. However $\sigma_w^2(x,z)/\sigma_{w,b}^2(z)$ shifts such that it is comparatively more aligned with Δu, which is consistent with the effects produced by the linearized wake production (see discussion in Section 2.5). It should be noted that this mechanism is entirely absent in rough-wall boundary layers on hills without canopies (Poggi and Katul 2008).

Why P_{wake} affects $\sigma_w^2(x,z)/\sigma_{w,b}^2(z)$ more than $\sigma_u^2(x,z)/\sigma_{u,b}^2(z)$ is possibly connected to the relative contributions of inactive eddy motion and background turbulence to the two velocity variances. A number of studies have already shown that wake production becomes a dominant source of energy in the vertical direction (Poggi et al. 2004a,b; Poggi and Katul 2006; Launiainen et al. 2007; Cava and Katul 2008) with inactive eddies and background turbulence playing a minor role (Poggi and Katul 2008). In the case of σ_u, shear production is the largest source of energy input, followed by inactive eddies and background turbulence, with wake production being only a minor source. Hence, inactive eddies may 'dilute' any effects of wake production on the phase relationships between σ_u and Δu.

When comparing the cross-correlation between $\Delta uw(x,z)/\overline{u'w'}_b(z)$ and σ_p and $\Delta uw(x,z)/\overline{u'w'}_b(z)$ and $\sigma_u^2(x,z)/\sigma_{u,b}^2(z)$ for the non-separating case, there is an anomalous shift between $\Delta uw(x,z)/\overline{u'w'}_b(z)$ and σ_p not detected in the inner or outer layer analysis, and is even more exaggerated in the separating LES run. This is perhaps suggestive that recirculation does not modify only the mean pressure gradient, but σ_p as well inside the canopy. This topic will be explored in a later section.

4.5.4 Lower Canopy Layer Scaling

Figure 13 shows the longitudinal variations of $\Delta u(x,z)/U_b(z)$, $\Delta uw(x,z)/\overline{u'w'}_b(z)$, $\sigma_u^2(x,z)/\sigma_{u,b}^2(z)$, and $\sigma_w^2(x,z)/\sigma_{w,b}^2(z)$ at the lower canopy layer reference level.

For the non-separating case, $\Delta uw(x,z)/\overline{u'w'}_b(z)$, $\sigma_u^2(x,z)/\sigma_{u,b}^2(z)$ and $\sigma_w^2(x,z)/\sigma_{w,b}^2(z)$ are almost in phase, and the shear-stress perturbations again explain almost 100% of the longitudinal variability in the two velocity variances.

For the separating case, $\Delta uw(x,z)/\overline{u'w'}_b(z)$ explains much of the variability in $\sigma_w^2(x,z)/\sigma_{w,b}^2(z)$. For the deeper canopy layers, wake production is small due to the small mean velocity, and shear production remains the main source of energy input for σ_w (with background turbulence and inactive eddies still playing a minor role). For σ_u, the relative importance of inactive eddies and shear production become comparable thereby inducing some de-correlation between the spatial variations in $\Delta uw(x,z)/\overline{u'w'}_b(z)$ and $\sigma_u^2(x,z)/\sigma_{u,b}^2(z)$. Hence, unlike the vertical velocity variance, there is no single scaling variable that explains the horizontal variations of both the longitudinal velocity and pressure variances.

4.6 Scaling Arguments for Pressure Variance

Figure 14 compares measured and modelled σ_p using Eq. 26 at all positions across the hill. This simplified scaling analysis correctly captures the order of magnitude of σ_p above the canopy but significantly underestimates its magnitude inside the canopy for both separating and non-separating runs. Again, Eq. 27 was not intended as a model to be validated in a one-to-one comparison. It only considered a primitive scaling argument for one of the source terms: the mean flow turbulent/interactions in the vertical. Hence, the fact that such a model provided a reasonable estimate of σ_p is rather encouraging and indicative that σ_p may be dominated by such mean-flow/turbulent interaction effects.

Interestingly, for the non-separating case, a quasi-linear relationship between measured and modelled σ_p still emerges inside the canopy. The intercept of such a linear relationship suggests that σ_p is finite inside the canopy even when the model (taken as a surrogate for the mean-flow turbulent interaction contribution) predicts a near-zero value. For the separating case, the relationship between measured and modelled σ_p inside the canopy is

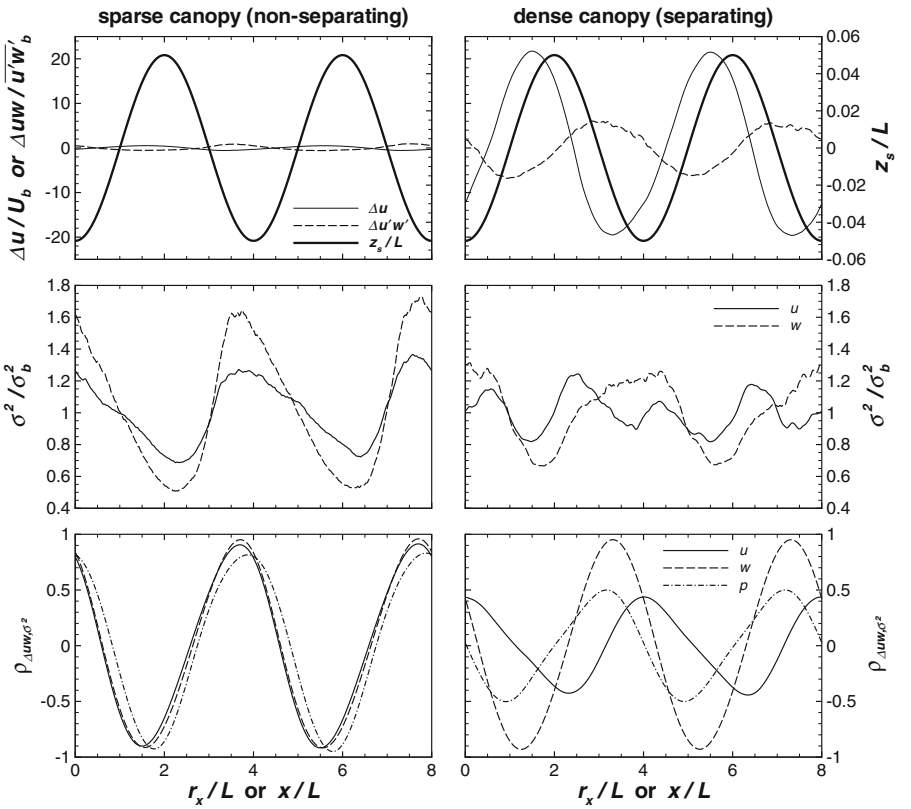

Fig. 13 Same as Fig. 12 but for the lower canopy instead of the upper canopy layer

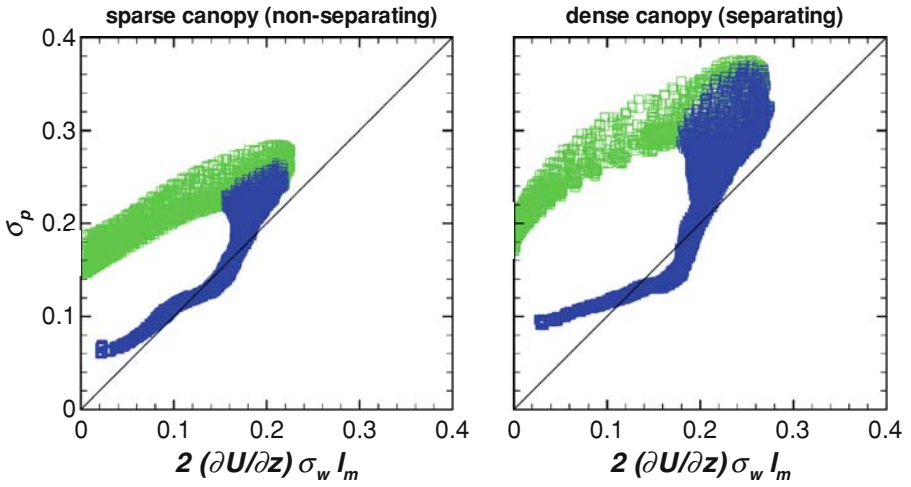

Fig. 14 Comparison between measured and modelled σ_p using Eq. 27 for all positions across the hill for the non-separating (*left*) and separating (*right*) cases. *Black symbols* indicate positions above the canopy while *red symbols* indicate positions within the canopy. The one-to-one line (*dashed*) is also shown for reference

clearly non-linear though the intercept appears comparable to the non-separating case. Hence, this analysis appears to suggest that the intercept is not very sensitive to leaf area density variation.

5 Summary and Conclusions

The impact of leaf area density variations on second-order statistics of the flow above a train of gentle hills covered with a tall canopy is explored via two LES runs. The hill surface in these LES runs is sufficiently gentle with a hill height comparable to the canopy height; two leaf area densities that differ by a factor of 10 are used. The analysis in FB04 regarding a critical leaf area density that induces recirculation is consistent with findings from these two LES runs. For a small leaf area density, no recirculation zone was predicted to occur by FB04, while for a dense canopy, a layer of reversed flow inside the canopy on the lee side of the hill was predicted. Both predictions agree with the two LES runs here and flume experiments reported by PK07. The emerging picture from this analysis regarding the effects of *increasing* leaf area density on the second-order flow statistics above a train of hills are as follows:

(1) Within the middle layer, zones of intense shear stress near the canopy-atmosphere system persist even further up than the predicted middle-layer level, which 'contaminates' some of the middle and outer layers with shear-stress gradients. The implications of these persistent shear-stress gradients is that RDT performs rather poorly for the dense canopy case when compared to its sparse-canopy counterpart, at least in reproducing the phase relationships between hill-induced perturbations in velocity variances and Δu. Some of these gradients are the result of the frictionless lid imposed on the LES runs at the top of the boundary layer.

(2) Within the inner layer, the phase relationships between the hill-induced spatial variations in the two velocity variances and the momentum flux is better reproduced by K-theory (at least when compared to the non-separating canopy run). This finding suggests that K-theory can be used to predict hill-induced perturbations (not absolute flow quantities) within the inner layer of a dense canopy.

(3) Within the canopy layer, the magnitude of wake production increases with increasing leaf area. This increase results in σ_w being more in phase with Δu than with the shear stress. However, background turbulence and inactive eddies may dampen the effect of wake production on producing such phase relationships between σ_u and Δu. It should be noted that this mechanism is entirely absent in rough-wall boundary layers above gentle hills. The increase in leaf area density weakens the strong phase relationships between σ_u and σ_w and the local shear stress observed for the low leaf area density case (for both upper and lower canopy levels).

An order-of-magnitude increase in leaf area density does not significantly affect the phase relationship between mean surface pressure and topography, though these LES results confirm that the minimum mean pressure is shifted downstream from the maximum topographic surface (see PK07 and RV05). The increase in leaf area density simply stretches this difference further downstream. The implications of this shift is to increase the pressure drag, the dominant term in the overall drag on the hill surface, by about 15%. With regards to pressure variance, it was shown that increasing leaf area density increases σ_p/u_*^2 near the canopy top, consistent with a primitive scaling argument on the leading term describing the mean-flow turbulent interaction. It is shown that this scaling argument leads to an order-of-magnitude

estimate of $\sigma_p \sim 2\sigma_w\sqrt{-\overline{u'w'}}$ above the canopy. Because topographic variability produces zones of intense shear stress in the dense canopy case, these zones are responsible for the increased σ_p near the canopy top. Inside the canopy, other processes are at play, and the proposed scaling argument here significantly underestimates σ_p.

The findings presented here shed light on the impact of canopy density variations on vegetation-orography flow interactions and subsequently on phase relationships of mean and turbulent statistics within the four key scaling regimes and with respect to the hill. It is anticipated that this understanding will aid in the development of simpler models representing this important feature of land-atmosphere interactions and will help guide measurement interpretation in this complex regime. Applications that can take advantage of these findings include (i) pressure-induced fluctuations in gas transfer from the soil pores to the forest floor (where σ_p is a key input), (ii) footprint models used to interpret micrometeorological flux and concentration measurements on complex terrain (where σ_w is a key input), (iii) three-dimensional Lagrangian trajectory models for scalars or particles (where the entire stress tensor and mean flow are needed), (iv) applications such as positioning wind turbines on complex terrain (where the entire stress tensor and mean flow are needed), and (iv) effective drag representation of the hill-canopy system in climate or other large-scale models (where phase shifts between topography and pressure is a key input).

Acknowledgements The authors are sincerely grateful to Peter Sullivan at NCAR for developing the backbone of NCAR's curvilinear LES code, and for many fruitful discussions. Numerous discussions with Keith Ayotte, John Finnigan and Stephen Belcher are also appreciated. E. G. Patton acknowledges support from the BEACHON program within NCAR's Institute of Integrative and Multidisciplinary Earth Sciences (TIIMES) and the Center for Multiscale Modeling of Atmospheric Processes (CMMAP) at Colorado State University, NSF grants ATM-0425247 and contract G-3045-9 to NCAR. G. G. Katul acknowledges travel support from TIIMES and NCAR's Mesoscale and Microscale Meteorology Division. Partial funding for G. Katul was also provided by the National Science Foundation (NSF-EAR-06-35787, NSF-EAR-06-28432, and NSF-ATM-0724088), the Binational Agricultural Research and Development fund (BARD), Research Grant No. IS3861-06. Computational time was provided both by NCAR and by NERSC (National Energy Research Scientific Computing Center which is supported by the Office of Science of the U.S. Department of Energy under Contract No. DE-AC02-05CH11231).

References

Athanassiadou M, Castro I (2001) Neutral flow over a series of rough hills: a laboratory experiment. Boundary-Layer Meteorol 101(1):1–30

Aubinet M, Heinesch B, Yarneaux M (2003) Horizontal and vertical CO_2 advection in a sloping forest. Boundary-Layer Meteorol 108:397–417

Aubinet M, Berbigier P, Bernhofer C, Cescatti A, Feigenwinter C, Granier A, Grunwald H, Havrankova K, Heinesch B, Longdoz B, Marcolla B, Montagnani L, Sedlak P (2005) Comparing CO_2 storage fluxes and advection at night at different CARBOEUROFLUX sites. Boundary-Layer Meteorol 116:63–94

Ayotte K (1997) Optimization of upstream profiles in modelled flow over complex terrain. Boundary-Layer Meteorol 83(2):285–309

Ayotte K, Hughes D (2004) Observations of boundary layer wind tunnel flow over isolated ridges of varying steepness and roughness. Boundary-Layer Meteorol 112:525–556

Belcher S, Hunt J (1998) Turbulent flow over hills and waves. Ann Rev Fluid Mech 30:507–538

Belcher S, Wood N (1996) Form and wave drag due to stably stratified turbulent flow over low ridges. Q J Roy Meteorol Soc 122(532, Part B):863–902

Beljaars A, Brown A, Wood N (2004) A new parametrization of turbulent orographic form drag. Q J Roy Meteorol Soc 130(599, Part B):1327–1347. doi:10.1256/qj.03.073

Besio S, Mazzino A, Ratto C (2001) Local law-of-the-wall in complex topography: a confirmation from wind tunnel experiments. Phys Lett A 282(4–5):325–330
Bitsuamlak G, Stathopoulos T, Bedard C (2004) Numerical evaluation of wind flow over complex terrain: review. J Aerosp Eng 17(4):135–145. doi:10.1061/(ASCE)0893-1321(2004)17:4(135)
Bitsuamlak G, Stathopoulos T, Bedard C (2006) Effects of upstream two-dimensional hills on design wind loads: a computational approach. Wind Struct 9(1):37–58
Britter R, Hunt J, Richards K (1981) Air-flow over a two-dimensional hill—studies of velocity speed-up, roughness effects and turbulence. Q J Roy Meteorol Soc 107(451):91–110
Brown A, Hobson J, Wood N (2001) Large-eddy simulation of neutral turbulent flow over rough sinusoidal ridges. Boundary-Layer Meteorol 98(3):411–441
Cava D, Katul GG (2008) Spectral short-circuiting and wake production within the canopy trunk space of an alpine hardwood forest. Boundary-Layer Meteorol 126(3):415–431. doi:10.1007/s10546-007-9246-x
Deardorff J (1980) Stratocumulus-capped mixed layers derived from a 3-dimensional model. Boundary-Layer Meteorol 18(4):495–527
Dupont S, Brunet Y, Finnigan J (2008) Large-eddy simulation of turbulent flow over a forested hill: Validation and coherent structure identification. Q J Roy Meteorol Soc 134:1911–1929. doi:10.1002/qj.328
Dwyer M, Patton E, Shaw R (1997) Turbulent kinetic energy budgets from a large-eddy simulation of airflow above and within a forest canopy. Boundary-Layer Meteorol 84(1):23–43
Feigenwinter C, Bernhofer C, Vogt R (2004) The influence of advection on short term CO_2 budget in and above a forest canopy. Boundary-Layer Meteorol 113:201–224
Finnigan J (2000) Turbulence in plant canopies. Ann Rev Fluid Mech 32:519–571
Finnigan J, Belcher S (2004) Flow over a hill covered with a plant canopy. Q J Roy Meteorol Soc 130(596, Part A):1–29. doi:10.1256/qj.02.177
Finnigan J, Shaw R (2008) Double-averaging methodology and its application to turbulent flows in above vegetation canopies. Acta Geophys 56(3):534–561. doi:10.2478/s11600-008-0034-x
Gong W, Ibbetson A (1989) A wind-tunnel study of turbulent-flow over model hills. Boundary-Layer Meteorol 49(1–2):113–148
Gong W, Taylor P, Dornbrack A (1996) Turbulent boundary-layer flow over fixed aerodynamically rough two-dimensional sinusoidal waves. J Fluid Mech 312:1–37
Grace J, Malhi Y (2002) Global change—carbon dioxide goes with the flow. Nature 416:594–595
Henn D, Sykes R (1999) Large-eddy simulation of flow over wavy surfaces. J Fluid Mech 383:75–112
Hunt J, Carruthers D (1990) Rapid distortion theory and the problems of turbulence. J Fluid Mech 212:497–532
Hunt J, Leibovich S, Richards KJ (1988) Turbulent shear flows over low hills. Q J Roy Meteorol Soc 114(484):1435–1470
Jackson P, Hunt J (1975) Turbulent wind flow over a low hill. Q J Roy Meteorol Soc 101(430):929–955
Katul G, Albertson J, Hsieh C, Conklin P, Sigmon J, Parlange M, Knoerr K (1996) The 'inactive' eddy motion and the large-scale turbulent pressure fluctuations in the dynamic sublayer. J Atmos Sci 53(17):2512–2524
Katul G, Porporato A, Nathan R, Siqueira M, Soons M, Poggi D, Horn H, Levin S (2005) Mechanistic analytical models for long-distance seed dispersal by wind. Am Nat 166(3):368–381
Katul G, Finnigan J, Poggi D, Leuning R, Belcher S (2006) The influence of hilly terrain on canopy-atmosphere carbon dioxide exchange. Boundary-Layer Meteorol 118(1):189–216. doi:10.1007/s10546-005-6436-2
Kim H, Lee C, Lim H, Kyong N (1997) An experimental and numerical study on the flow over two-dimensional hills. J Wind Eng Ind Aerodyn 66(1):17–33
Launiainen S, Vesala T, Molder M, Mammarella I, Smolander S, Rannik U, Kolari P, Hari P, Lindroth A, Katul G (2007) Vertical variability and effect of stability on turbulence characteristics down to the floor of a pine forest. Tellus 59B(2):919–936
Massman W (1997) An analytical one-dimensional model of momentum transfer by vegetation of arbitrary structure. Boundary-Layer Meteorol 83(3):407–421
Nathan R, Katul G (2005) Foliage shedding in deciduous forests lifts up long-distance seed dispersal by wind. Proc Natl Acad Sci 102(23):8251–8256. doi:10.1073/pnas.0503048102
Nathan R, Katul G, Horn H, Thomas S, Oren R, Avissar R, Pacala S, Levin S (2002) Mechanisms of long-distance dispersal of seeds by wind. Nature 418:409–413
Patton EG, Sullivan PP, Ayotte KW (2006) Turbulent flow over isolated ridges: influence of vegetation. In: 17th symposium on boundary layers and turbulence, San Diego, CA, J6.12. http://ams.confex.com/ams/pdfpapers/110925.pdf
Poggi D, Katul GG (2006) Two-dimensional scalar spectra in the deeper layers of a dense and uniform model canopy. Boundary-Layer Meteorol 121(2):267–281. doi:10.1007/s10546-006-9075-3
Poggi D, Katul G (2007a) The ejection-sweep cycle over bare and forested gentle hills: a laboratory experiment. Boundary-Layer Meteorol 122(3):493–515. doi:10.1007/s10546-006-9117-x

Poggi D, Katul GG (2007b) An experimental investigation of the mean momentum budget inside dense canopies on narrow gentle hilly terrain. Agric For Meteorol 144(1–2):1–13. doi:10.1016/j.agrformet.2007.01.009
Poggi D, Katul GG (2007c) Turbulent flows on forested hilly terrain: The recirculation region. Q J Roy Meteorol Soc 133(625, Part B):1027–1039. doi:10.1002/qj.73
Poggi D, Katul G (2008) Turbulent intensities and velocity spectra for bare and forested gentle hills: Flume experiments. Boundary-Layer Meteorol 129(3):24–46
Poggi D, Katul G, Albertson J (2004a) Momentum transfer and turbulent kinetic energy budgets within a dense model canopy. Boundary-Layer Meteorol 111(3):589–614
Poggi D, Porporato A, Ridolfi L, Katul G, Albertson J (2004b) The effect of vegetation density on canopy sublayer turbulence. Boundary-Layer Meteorol 111(3):565–587
Poggi D, Katul GG, Albertson JD, Ridolfi L (2007) An experimental investigation of turbulent flows over a hilly surface. Phys Fluids 19(3). doi:10.1063/1.2565528
Poggi D, Katul GG, Finnigan JJ, Belcher SE (2008) Analytical models for the mean flow inside dense canopies on gentle hilly terrain. Q J Roy Meteorol Soc 134(3):1095–1112
Raupach M (1994) Simplified expressions for vegetation roughness length and zero-plane displacement as functions of canopy height and area index. Boundary-Layer Meteorol 71(1–2):211–216
Raupach M, Finnigan J (1997) The influence of topography on meteorological variables and surface–atmosphere interactions. J Hydrol 190(3–4):182–213
Raupach M, Shaw R (1982) Averaging procedures for flow within vegetation canopies. Boundary-Layer Meteorol 22(1):79–90
Raupach M, Thom A (1981) Turbulence in and above plant canopies. Ann Rev Fluid Mech 13:97–129
Raupach M, Weng W, Carruthers D, Hunt J (1992) Temperature and humidity fields and fluxes over low hills. Q J Roy Meteorol Soc 118(504, Part B):191–225
Raupach M, Finnigan J, Brunet Y (1996) Coherent eddies and turbulence in vegetation canopies: The mixing-layer analogy. Boundary-Layer Meteorol 78(3–4):351–382
Ross A (2008) Large eddy simulations of flow over forested ridges. Boundary-Layer Meteorol 128(1):59–76
Ross A, Vosper S (2005) Neutral turbulent flow over forested hills. Q J Roy Meteorol Soc 131(609, Part A):1841–1862. doi:10.1256/qj.04.129
Salvetti M, Damiani R, Beux F (2001) Drag prediction over steep sinusoidal wavy surfaces. Phys Fluids 13(9):2728–2731
Schmid H (2002) Footprint modeling for vegetation atmosphere exchange studies: a review and perspective. Agric For Meteorol 113:159–183
Shaw R, Patton E (2003) Canopy element influences on resolved- and subgrid-scale energy within a large-eddy simulation. Agric For Meteorol 115(1–2):5–17
Staebler R, Fitzjarrald D (2004) Observing subcanopy CO_2 advection. Agric For Meteorol 122:139–156
Sullivan P, Edson J, Hristov T, McWilliams J (2008) Large eddy simulations and observations of atmospheric marine boundary layers above non-equilibrium surface waves. J Atmos Sci 65:1225–1245
Tamura T, Okuno A, Sugio Y (2007) LES analysis of turbulent boundary layer over 3D steep hill covered with vegetation. J Wind Eng Ind Aerodyn 95(9–11):1463–1475. doi:10.1016/j.jweia.2007.02.014
Taylor P (1998) Turbulent boundary-layer flow over low and moderate slope hills. J Wind Eng Ind Aerodyn 74(6):25–47
Tennekes H, Lumley J (1972) A first course in turbulence. MIT Press, Cambridge, 300 pp
Vosper SB, Brown AR (2007) The effect of small-scale hills on orographic drag. Q J Roy Meteorol Soc 133(627, Part B):1345–1352. doi:10.1002/qj.101
Wagner C, Kuhn S, von Rohr PR (2007) Scalar transport from a point source in flows over wavy walls. Exp Fluids 43(2–3):261–271. doi:10.1007/s00348-007-0340-0
Williams C, LaDeau S, Oren R, Katul G (2006) Modeling seed dispersal distances: implications for transgenic Pinus taeda. Ecol Appl 16(1):117–124
Wood N (2000) Wind flow over complex terrain: A historical perspective and the prospect for large-eddy modelling. Boundary-Layer Meteorol 96(1–2):11–32
Xu D, Taylor P (1995) Boundary-layer parametrization of drag over small-scale topography. Q J Roy Meteorol Soc 121(522, Part B):433–443
Yaglom A (1979) Similarity laws for constant-pressure and pressure gradient turbulent wall flows. Ann Rev Fluid Mech 11:505–540
Ying R, Canuto V (1996) Turbulence modelling over two-dimensional hills using an algebraic Reynolds stress expression. Boundary-Layer Meteorol 77(1):69–99